THE SYMBIOTIC NEUTRON STAR BINARY GX 1+4/V2116 OPHIUCHI

Deepto Chakrabarty[1]
Center for Space Research, Massachusetts Institute of Technology, Cambridge, MA 02139;
deepto@space.mit.edu

and

Paul Roche
Astronomy Centre, University of Sussex, Brighton BN1 9QH, England, UK; pdr@star.maps.susx.ac.uk

Submitted March 10, 1997; revised May 30, 1997
Accepted for publication in The Astrophysical Journal

ABSTRACT

We present extensive optical, infrared, and X-ray observations of the S-type symbiotic low-mass X-ray binary GX 1+4/V2116 Oph, which consists of a 2-min X-ray pulsar accreting from an M6 III giant. This is the only symbiotic system definitely known to contain a neutron star. The mean observed spectral type of the X-ray-heated mass donor is M5 III. The steady interstellar extinction toward the binary ($A_V = 5.0 \pm 0.6$) contrasts the variable hydrogen column density inferred from X-ray measurements, most likely evidence for a variable stellar wind. The mass donor is probably near the tip of the first-ascent red giant branch, in which case the system is 3–6 kpc distant and has an X-ray luminosity of $\sim 10^{37}$ erg s^{-1}. It is also possible, though less likely, that the donor star is just beginning its ascent of the asymptotic giant branch, in which case the system is 12–15 kpc distant and has an X-ray luminosity of $\sim 10^{38}$ erg s^{-1}. However, our measured A_V argues against such a large distance.

We show that the dense ($N_e \sim 10^9$ cm^{-3}) emission-line nebula enshrouding the binary is powered by ultraviolet radiation from an accretion disk. The emission-line spectrum constrains the temperature profile and inner radius of the disk (and thus the pulsar's magnetic field strength), and we mention the implications this has for explaining the accretion torque reversals observed in the pulsar. We also show that the binary period must be $\gtrsim 100$ d and is most likely $\gtrsim 260$ d, making GX 1+4 the only known low-mass X-ray binary with $P_{\rm orb} > 10$ d. If

[1]NASA Compton GRO Postdoctoral Fellow

the mass donor fills its Roche lobe, the mass transfer rate must be highly super-Eddington, requiring considerable mass loss from the binary. We discuss the alternative possibility that the accretion disk forms from the slow, dense stellar wind expected from the red giant.

Subject headings: accretion, accretion disks — binaries: symbiotic — pulsars: individual: GX 1+4 — stars: individual: V2116 Oph — stars: neutron — X-rays: stars

1. INTRODUCTION

Low-mass X-ray binaries (LMXBs) with evolved giant donors are the current state or probable progenitor of most low-mass neutron star binaries with wide ($P_{\rm orb} \gtrsim 2$ d) orbital separations (see Verbunt & van den Heuvel 1995 for a review). In the usual scenario, mass transfer onto the neutron star begins when its low mass companion ascends the giant branch and fills its Roche lobe. This mass transfer, driven by the nuclear evolution and expansion of the giant, continues at a high rate until the donor envelope is exhausted, eventually leaving a wide white dwarf/neutron star binary. Tidal torques exerted by the red giant envelope act rapidly to circularize the orbit.

Many examples of systems which probably evolved in this way are known. Among current LMXBs, Cyg X-2 and 2S 0921–63 are in long-period (~ 9 d) orbits with moderately evolved (F or G type) giants, and the recently discovered bursting X-ray pulsar GRO J1744–28 is in a wide, 11.8-d circular orbit suggestive of tidal interactions with a giant companion (Finger et al. 1996). There are over 30 known low-mass binary radio pulsars in wide circular orbits whose white dwarf companions are probably the remnant core of a red giant whose envelope was exhausted or ejected during mass transfer (Phinney & Kulkarni 1994; Camilo 1995). However, some of these radio pulsar binaries have orbital periods much longer ($P_{\rm orb} \gg 10$ d) than the widest known LMXBs. The presumed progenitors of such systems, LMXBs accreting from highly evolved (K or M type) giant donors, have not been previously identified. They are expected to be rare, owing to the short duration of both the K/M giant lifetime and the highly unstable mass transfer stage expected for Roche-lobe-overflow LMXBs with $P_{\rm orb} \gtrsim 2$ d (Kalogera & Webbink 1996). The high mass transfer rate might even smother the X-ray emission, making the system unobservable as an LMXB.

If such a system were observed, it would almost certainly be classified as symbiotic binary. These consist of a K/M giant primary and a hot secondary enshrouded by an emission line nebula, which results from photoionization of the red giant's wind by the secondary (see

Kenyon 1986 and Iben & Tutukov 1996 for reviews). Their observational characteristic is a composite spectrum in which strong emission lines are superimposed on the cool molecular absorption spectrum of the highly evolved primary. Over 100 symbiotic binaries are known, most of which have hot main sequence or white dwarf secondaries. The only symbiotic known to have a neutron star companion is the X-ray pulsar binary GX 1+4/V2116 Oph (Davidsen, Malina, & Bowyer 1977), although the X-ray binary 4U 1700+24/HD 154791 (Garcia et al. 1983) may be a second example. No other LMXBs with M giant companions are known. GX 1+4 is thus a promising candidate progenitor for the widest low-mass neutron star binaries (e.g., Taam & van den Heuvel 1986).

The $\sim$ 2 min accretion-powered binary pulsar GX 1+4 (= 4U 1728–247) was discovered in a hard X-ray balloon observation over 25 years ago (Lewin, Ricker, & McClintock 1971). Throughout the 1970s, it was the brightest hard X-ray source in the Galactic center region ($\sim$50–200 mCrab), and the pulsar was spinning up at a rapid rate ($|\nu/\dot{\nu}| \approx 40$ yr). In the early 1980s GX 1+4 entered an extended low state, with soft X-ray flux of < 0.5 mCrab (Hall & Davelaar 1983; Mukai 1988). When it reemerged with low luminosity ($\sim$ 2 mCrab) in 1987, the pulsar was spinning down rapidly at nearly the same rate that it had been spinning up previously (Makishima et al. 1988). GX 1+4 spun down and gradually brightened to $\sim$100 mCrab until 1994, when it briefly resumed rapid spin-up before returning to a spin-down state (Chakrabarty et al. 1997). If interpreted in terms of standard magnetic accretion torque theory for X-ray pulsars accreting from disks, (e.g., Ghosh & Lamb 1979), these torque reversals imply an extraordinarily strong ($\sim 10^{14}$ G) dipole magnetic field at the surface of the neutron star.

Shortly after its discovery, GX 1+4 was identified with the bright infrared source V2116 Oph (Glass & Feast 1973). Optical spectroscopy of this star clearly established it as a symbiotic (Davidsen et al. 1977). In addition to a number of very bright emission lines due to H I (especially Hα) and He I, the optical spectrum also contained emission lines of several highly ionized species, notably [Fe VII] and [Fe X]. This indicated the presence of high-energy ionizing photons, suggesting that the hot secondary was a compact object and thus strengthening the association with GX 1+4. Optical pulsations consistent with the spin period of GX 1+4 have recently been detected from V2116 Oph (Jablonski et al. 1997).

In this paper, we present extensive observations of the GX 1+4/V2116 Oph system at optical, infrared, and X-ray wavelengths.

2. OBSERVATIONS

2.1. X-ray observations

The pulsed hard X-ray (20–60 keV) emission from GX 1+4 has been observed continuously since 1991 April with the BATSE all-sky monitor on the *Compton Gamma Ray Observatory*. These observations are described in detail elsewhere (Chakrabarty et al. 1994, 1997). However, to provide context for the multiwavelength observations presented in this paper, Table 1 lists the 20–60 keV pulsed intensity of GX 1+4 measured by BATSE for the times of each of the post-1991 multiwavelength observations described in this paper. The hard X-ray pulsed intensities are excerpted from a BATSE pulsed flux history given by Chakrabarty (1996). It should be emphasized that these intensities represent only the pulsed component of the emission above 20 keV. Although the extent to which the BATSE pulsed intensity is a precise tracer of the bolometric flux from GX 1+4 remains an open question (Chakrabarty et al. 1997), we will treat it as an approximate tracer in this paper.

We obtained two 0.1–2.4 keV observations of the GX 1+4 field with the *ROSAT* High Resolution Imager (HRI). The first observation was for a total of 4894 s on 1995 March 12–16. No point sources were detected in the field of view. The 95%-confidence upper limit on emission from GX 1+4 was 0.0029 count s^{-1}.

A second observation was made for a total of 5861 s on 1996 March 26–28. A total of 305 ± 17 counts was detected from GX 1+4, corresponding to an intensity of 0.0506 ± 0.0030 count s^{-1} with a pulsed fraction of approximately 70%. The derived coordinates of GX 1+4 with respect to the J2000.0 equinox are: RA = $17^{\rm h}\,32{\rm m}\,02\overset{\rm s}{.}31$, Dec = $-24^\circ\,44'\,44\overset{''}{.}10$. The 90%-confidence error circle due to photon statistics and the point-spread function of the instrument has radius 0.8 arcsec. There is an additional 6.3 arcsec (1σ) systematic uncertainty in the *ROSAT* attitude solution, resulting in an overall 90%-confidence error circle radius of 10.4 arcsec. The center of our error circle lies within 4 arcsec of the optical coordinates of V2116 Oph. It also lies within 3 arcsec of the center of an earlier 11.4-arcsec-radius (90%-confidence) *ROSAT*/PSPC position determined from only 15 counts (Predehl, Friedrich, & Staubert 1995). The azimuthally-averaged surface brightness profile of the GX 1+4 region shows no evidence for the faint, diffuse halo reported by Predehl et al. (1995).

2.2. Optical astrometry and optical/IR photometry

Optical astrometry of the GX 1+4 field was obtained using plate J2333 from the SERC(J) southern sky survey, exposed at the UK Schimdt Telescope in Australia on 1976 May 27. Astrometric coordinates for V2116 Oph and several neighboring stars, precessed to the J2000.0 equinox, are given in Table 2. An *R*-band finder image of the field, shown in

Figure 1, was acquired on 1993 September 10 with the $f/11$ Nasymth EMMI camera on the 3.5-m New Technology Telescope (NTT) at the European Southern Observatory (ESO) in La Silla, Chile. The 90% confidence *ROSAT* error circle derived above for the X-ray source is also shown.

Deep optical CCD photometry was obtained on 1993 June 29 using the $f/2.8$ prime focus COSMIC camera on the 5-m Hale telescope at Palomar Mountain, California. The B (4400 Å), V (5500 Å), and R (7000 Å) magnitudes of V2116 Oph are given in Table 2. To aid future differential photometry, the magnitudes for several field stars are given as well. Infrared photometry in the J (1.25 μm), H (1.65 μm), and K (2.2 μm) bands was obtained during 1993–1995 using the the $f/50$ Cassegrain Mk III infrared photometer on the SAAO 1.9-m Radcliffe telescope; the infrared camera (IRCAM) on the 3.8-m United Kingdom Infrared Telescope (UKIRT) at Mauna Kea, Hawaii; and the continuously-variable filter photometer (CVF) on the 1.5-m Telescopio Carlos Sanchez (TCS) at the Teide Observatory in Izaña, Tenerife, Canary Islands, Spain. In some of the SAAO observations, L (3.6 μm) band measurements were also acquired, and several L' (3.7 μm) band measurements were obtained during the UKIRT observations. The complete infrared photometric history of V2116 Oph, including all previously published measurements, is summarized in Table 3.

2.3. Optical/IR spectroscopy

Spectroscopic observations of V2116 Oph were obtained on 1991 August 8–9 and 1993 June 30 using the $f/15.7$ Cassegrain double spectrograph of the Palomar 5m Hale telescope. A service observation was made during a bright X-ray outburst of GX 1+4 on 1993 September 10, using the $f/11$ Nasmyth EMMI spectrograph on the 3.5-m New Technology Telescope (NTT) of the European Southern Observatory (ESO) in Cerro La Silla, Chile. This observation, made with EMMI in its red imaging and low dispersion (RILD) mode, was acquired during an engineering night, and a significant part of the beam was obscured leading to a rather low count rate; however, the obscuration was identical for all the data acquired.

Several archival observations are available from the 3.9-m Anglo-Australian Telescope (AAT) at Siding Spring Mountain, New South Wales, Australia. Spectra were acquired on 1976 April 10 and 1976 August 20 using the Boller and Chivens spectrograph and the IDS detector. The 1976 August spectrum was previously published by Whelan et al. (1977). An additional observation was obtained on 1984 April 22, during the X-ray low state of GX 1+4 reported by *EXOSAT*. More recently, two AAT service observations were made on 1993 September 10 using the $f/8$ Cassegrain RGO spectrograph. We obtained a high-resolution

Hα observation with this spectrograph on 1994 February 26.

An Hα spectrum was also obtained on 1993 July 1 using the $f/11$ ISIS double spectrograph on the 4.2-m William Herschel telescope at the Roque de los Muchachos Observatory in La Palma, Canary Islands, Spain. Several additional Hα observations were obtained during 1993–1995 using the $f/18$ Cassegrain image tube spectrograph and Reticon detector on the 1.9-m Radcliffe telescope of the South African Astronomical Observatory (SAAO) in Sutherland, Cape Province, South Africa.

All of the optical spectra were reduced using the Figaro analysis package (Shortridge 1991). Where suitable spectrophotometric standards were observed, the data were flux-calibrated and corrected for atmospheric extinction. We corrected the observed wavelengths for the Earth's motion with respect to the solar system barycenter.

A summary of all known optical spectroscopic observations of V2116 Oph, including previously published measurements, is given in Table 4. Representative wide coverage spectra are shown in Figure 2. A more detailed medium-resolution spectra is shown in Figure 3.

Low-resolution ($\lambda/\Delta\lambda \sim 150$) infrared grism spectroscopy of V2116 Oph in the JHK bands were obtained on 1993 April 6 with the $f/70$ Cassegrain infrared camera and a 58×62 InSb array on the Palomar 5-m Hale telescope. These spectra were obtained using a 1 arcsec slit and broad-band JHK filters for order sorting. Instrumental and atmospheric absorption features were removed using the featureless continuum of the G0 V star HR 4345 (see Graham et al. 1992 for details).

3. RESULTS

3.1. Spectral classification

Davidsen et al. (1977) assigned a tentative classification of M6 III to V2116 Oph, warning that "in view of the complicated nature of the spectrum, this preliminary estimate should be accepted with caution." We have several available spectra which include the $\lambda\lambda$7300–8100 range and thus are suitable for checking the classification. A visual comparison of the near-infrared spectra in Figure 2 with the M giant spectral sequences of Kirkpatrick et al. (1991) confirm that the star is mid to late M class, in particular by means of the TiO and VO absorption bands, which are sensitive to temperature in M giants. Kenyon & Fernandez-Castro (1987) and Terndrup et al. (1990) have defined absorption indices to measure the depth of these features relative to the interpolated continuum. The $I(6180)$=[TiO]$_1$ and $I(7100)$=[TiO]$_2$ indices of Kenyon & Fernandez-Castro (1987) and the $S(7890)$ index of

Terndrup et al. (1990) measure the depth of the TiO features, while the $I(7865)$=[VO] (Kenyon & Fernandez-Castro 1987) and $I(7450)$ (Terndrup et al. 1990) indices measure VO absorption. All of these indices have been extensively calibrated against spectral type using a large number of K and M giants and supergiants and are relatively insensitive to reddening.

When measuring these indices in V2116 Oph, we found that the two TiO indices of Kenyon & Fernandez-Castro gave spurious results, measuring negligible TiO $\lambda\lambda$6180, 7100 absorption (typical of K and early M stars) despite the obvious presence of stronger features at longer wavelengths. Since this is probably due to contamination of the red giant absorption spectrum by nebular emission or an accretion disk, we confined our analysis to the other three absorption indices at longer wavelengths, which all give consistent results (see Table 5). The 1975 August, 1984 April, and 1993 June spectra are all consistent with an M5 star, but the 1993 September 10 spectrum indicates a somewhat higher temperature, around M3.

CO absorption strength in late type stars is correlated with both luminosity and effective temperature (e.g., Kleimann & Hall 1986). Doyon et al. (1994) quantified this relationship in terms of a spectroscopic index for CO absorption at 2.3 μm. Using our measurement of this feature in the 1993 April Palomar data (Figure 4), we find $[\mathrm{CO}]_{\mathrm{sp}}$=0.31, which clearly identified V2116 Oph as luminosity class III. High-resolution infrared spectroscopy of the CO absorption band features may be able to place more quantitative constraints on the luminosity.

X-ray heating is probably responsible for our M3 measurement on 1993 September 10. Data from the BATSE all-sky monitor on the *Compton Gamma Ray Observatory* indicate that the hard X-ray (20–60 keV) pulsed flux from GX 1+4 on 1993 September 10 was a factor of 3 higher than on 1993 June 30 (see Table 1). If we assume that the BATSE measurements are a tracer of the bolometric luminosity of GX 1+4 and that the temperature change is due to a change in the X-ray heating of the red giant photosphere between the two observations, then we can write

$$T_{\mathrm{M3}}^4 - \frac{3L_x f \alpha}{2\pi\sigma R_g^2} = T_{\mathrm{M5}}^4 - \frac{L_x f \alpha}{2\pi\sigma R_g^2}, \qquad (1)$$

where T_{M3}=3675 K and T_{M5}=3470 K are the effective temperatures for the red giant (Dyck et al. 1996), R_g is the red giant radius, L_x is the X-ray luminosity in "quiescence" (that is, on 1993 June 30), α is the X-ray albedo of the red giant, f is the fraction of L_x intercepted by the red giant surface, and $\sigma = 5.67\times10^{-5}$ erg cm^{-2} K^{-4} s^{-1} is the Stefan-Boltzman constant. For a neutron star/red giant binary, we estimate $f \approx 0.03$ (e.g., Webbink, Rappaport, & Savonije 1983). Then, assuming $\alpha = 0.5$, we find that $L_x = 10^{37}\, R_{100}^2$ erg s^{-1}, where R_{100} is the red giant radius in units of $100R_\odot$. This calculation suggests that the effective temperature of the *unheated* red giant is $\approx$ 3370 K (corresponding to an M6 III star; Dyck et al. 1996), even though the mean *observed* spectral type is M5 III. However, the calculation should be treated

with caution; the X-rays may only ionize the red giant's atmosphere without penetrating to the photosphere (see, e.g., Proga et al. 1996). Further correlative study of the M giant's temperature and optical line profile variations with changing X-ray illumination may help clarify this point.

As a crude consistency check on our classification, we can use our infrared photometry to compute a color temperature. Fitting our 1993 April *JHKL* photometry to a reddened ($A_V = 5$; see below) blackbody, we find $T_{\rm color} = 2590$ K, which corresponds to an M6 III star (Ridgway et al. 1980). The resulting blackbody curve is compared with our low-resolution infrared spectra in Figure 4. The significant difference between our estimates of $T_{\rm color}$ and $T_{\rm eff}$, as well as the strong H-band excess above a reddened blackbody curve, can be understood in terms of the complicated near-infrared molecular opacities in the atmospheres of cool stars (Tsuji 1966; Wing 1981).

Infrared photometry may also be used to further classify symbiotic stars into one of two groups: the S-type ("stellar") symbiotics, whose IR colors are consistent with a late type giant; and the D-type ("dusty") symbiotics, where the cool star is usually a Mira variable and whose IR colors indicate the presence of even cooler dust emission (Webster & Allen 1975; Allen 1982; Munari et al. 1992). The *JHKL* colors of V2116 Oph fall close to the boundary of the two groups, but are most consistent with an S-type classification.

3.2. Reddening and column density

The optical colors of V2116 Oph are clearly inconsistent with those of an M giant for any amount of interstellar reddening, suggesting that much of the optical continuum is dominated by disk or nebular emission. Moreover, the H I Balmer and He I line ratios are also inconsistent with recombination in a standard "case B" radiative nebula (i.e. optically thick in the H I Lyman lines; Baker & Menzel 1938; Osterbrock 1989) for any amount of reddening, as is often seen in regions of high density and optical depth (Osterbrock 1989). Following Davidsen et al. (1977), we instead employed the infrared colors to determine the reddening.

Care must be taken to measure both the spectral type and the infrared colors simultaneously, since the temperature-dependence of M giant intrinsic colors on a JHK color-color diagram (Bessell & Brett 1988) parallels the interstellar reddening vector (Rieke & Lebofsky 1985). Fortunately, on two of the dates for which we have spectral classifications (1993 June 30 and 1993 September 10), we also obtained JHK photometry. Comparing the measured JHK colors on these dates with the intrinsic colors for M5 III and

M3 III giants, respectively (Bessell & Brett 1988), and assuming the reddening is constant over time, we find mean infrared color excesses of $\langle E(J-H)\rangle = 0.53 \pm 0.03$ and $\langle E(H-K)\rangle = 0.33 \pm 0.03$. Then, using the interstellar reddening law of Rieke & Lebofsky (1985), we infer that $E(B-V) = 1.63 \pm 0.19$, $A_V = 5.0 \pm 0.6$, and $A_K = 0.56 \pm 0.08$. The error bars for the last three quantities include the systematic uncertainty in the interstellar extinction law in addition to the measurement errors.

The stability of the infrared colors indicates that the observed extinction is constant, and thus probably interstellar in origin. Using the empirically measured relationship between optical extinction and interstellar X-ray absorption (Gorenstein 1975), we would expect a similarly constant hydrogen column density to the source of $N_{\rm H} \approx 1 \times 10^{22}$ cm^{-2}. However, archival X-ray spectral measurements of the column density have found substantial variability (e.g. Becker et al. 1976), but with a typical value of $N_{\rm H} \approx 4 \times 10^{22}$ cm^{-2}. At the same time, the inferred unabsorbed X-ray continuum shape has been fairly constant. It is interesting to note that our two *ROSAT* observations of GX 1+4, separated by a year, found an order of magnitude difference in the 0.1–2.4 keV intensity despite a difference of only 25% in the 20–60 keV intensity measured simultaneously by BATSE. The flux measured in the *ROSAT* band is extremely sensitive to the hydrogen column density. Our 1996 March *ROSAT* measured intensity is consistent with the level using the PIMMS simulation program[2] assuming the column density ($N_{\rm H} = 4 \times 10^{22}$ cm^{-2}) and spectral shape measured by *Rossi X-Ray Timing Explorer* in 1996 February (W. Cui 1996, priv. communication), and using the simultaneous BATSE 20–60 keV measurement for normalization. The 1995 March *ROSAT* non-detection is consistent with a higher column density $\gtrsim 7 \times 10^{22}$ cm^{-2}, well within the range of observed column density variability in GX 1+4. We conclude that the observed optical extinction is mainly due to interstellar dust, while the variable X-ray absorption is caused by gas local to GX 1+4, probably the wind of the red giant.

3.3. Emission line spectrum

We used our extinction estimate to compute the dereddened emission line fluxes $I(\lambda) = F(\lambda)e^{A(\lambda)/1.086}$ for each of our observations, where $F(\lambda)$ is the observed emission line flux and $A(\lambda)$ is the extinction in magnitudes as a function of wavelength. To compute $A(\lambda)$, we fit a cubic polynomial to the interstellar extinction law of Rieke & Lebofsky (1985):

[2]PIMMS (Portable, Interactive, Multi-Mission Simulator) is a tool for predicting count rates in X-ray astronomy missions for a variety of source spectral models. It was written by Koji Mukai at NASA/Goddard Space Flight Center and is available on the World Wide Web via anonymous FTP at `ftp://legacy.gsfc.nasa.gov/software/tools`.

$[A(\lambda)/A_V] = 0.01472 + 0.01425(1/\lambda) + 0.49011(1/\lambda)^2 - 0.10709(1/\lambda)^3$, where the wavelength λ is measured in microns. This fit is valid over the range 0.3 μm $< \lambda <$ 5 μm. The resulting dereddened emission line fluxes are included in Tables 6, 7, and 8. Table 6 contains a selected line list for the archival spectra from 1974–1988 as well as the 1993 June Palomar spectrum. Tables 7 and 8 contains detailed line lists for our observations on 1991 August 8 and 1993 September 10, respectively. The optical emission line features were identified using the tables of Meinel, Aveni, & Stockton (1975).

The dominant feature in all of the optical spectra is a tremendous Hα emission line. He I lines are also detected in all of the spectra. Very few forbidden lines are observed, indicating a high electron density in the emission line region. The 1991 August data from Palomar (Figure 3) provide the first high signal-to-noise measurement of the blue-end spectrum of V2116 Oph, revealing several hydrogen Balmer lines as well as weak emission from He II λ4686 and numerous other species. Three spectra were obtained on 1993 September 10 during a bright X-ray flare from GX 1+4. The ESO/NTT spectrum (bottom panel of Figure 2) extends into the near infrared, measuring the strong Ca II triplet and the extraordinarily strong O I λ8446 line, as well as a number of weaker lines from the hydrogen Paschen series. In the low-resolution infrared spectra (Figure 4), the H I Paβ and Brγ lines are detected.

A broad emission feature near λ6830 is present in the older spectra (1974–1988) and is weakly detected in the 1991 August spectrum. This feature, which is believed to arise from Raman scattering of O VI $\lambda\lambda$1032, 1038 by neutral hydrogen (Schmid 1989), is in general only observed in those symbiotic stars which have highly excited species like [Fe VII] (Allen 1980). Indeed, the [Fe VII] features reported by Davidsen et al. (1977) and detected in the 1976–1988 spectra are undetected in the more recent (1991–1995) spectra, consistent with the correspondingly weaker λ6830 emission.

The presence of numerous Fe II lines combined with the absence of any Fe III features indicates that the electron temperature $T_e < 30000$ K (Osterbrock 1989), so that the rich emission line spectrum we observe must be due to photoionization rather than collisional ionization or shock heating. Since a strong X-ray source (the pulsar) is present in the system, it is essential to determine whether the emission lines are primarily powered by ultraviolet photons (as in typical symbiotic binaries) or X-rays, since the ionization structure in the two cases will be quite different. By analogy with emission-line galaxies, we can use the location of the dereddened line ratios I([O III] λ5007)/I(Hβ) and I([O I] λ6300)/I(Hα) on a so-called BPT diagram (Baldwin, Phillips, & Terlevich 1981; Veilleux & Osterbrock 1987) to probe the nature of the photoionizing continuum. Emission-line galaxies known to be photoionized by ultraviolet radiation from OB stars populate a distinct region of these diagrams from those ionized by an X-ray continuum. The location of V2116 Oph on such a

diagram suggests that the nebula is ionized by thermal ultraviolet radiation rather than the non-thermal X-ray power law continuum expected from an accreting neutron star.

This being the case, we can apply the standard optical emission line diagnostics used for estimating the physical conditions in symbiotic nebulae. Following Iijima (1981), we used the dereddened line strengths of Hβ, He I λ4471, and He II λ4686 to estimate that the hot component of this symbiotic binary has a characteristic temperature $T_{\rm hot} \lesssim 90000$ K. (This estimate is an upper limit because the Hβ line may be depressed by optical depth effects; see Kenyon 1986 and the discussion below.) The ionizing source is much hotter than the photosphere of the M giant but considerably cooler than the characteristic temperature of the accreting neutron star. We conclude that the ionization source is an accretion disk around GX 1+4, which we discuss further in Section 4.3.

As noted by Davidsen et al. (1977), the large Hα/Hβ ratio indicates a high electron density and optical depth, leading to significant Balmer line self-absorption effects. Our 1991 August spectrum measures the Balmer decrement using the first six Balmer lines, providing a significant constraint on the physical conditions of the emission nebula. Comparing the measured ratios to models of a photoionized high-density slab of hydrogen (Drake & Ulrich 1980), we find they are consistent with electron temperature $T_e = 2 \times 10^4$ K, electron density $N_e \approx 10^9$ cm^{-3}, optical depths $\tau_{{\rm Ly}\alpha} \approx 10^6$ and $\tau_{{\rm H}\alpha} \approx 800$ in Lyα and Hα, and photoionization rate

$$R_{1C} \equiv 4\pi \int_{\nu_1}^{\infty} a_1(\nu) \frac{I_\nu}{h\nu} d\nu = 0.03 \ {\rm s}^{-1}, \tag{2}$$

where I_ν is the specific intensity of the external radiation field, $a_1(\nu)$ is the bound-free cross-section of the hydrogen ground state, $h = 6.6 \times 10^{-27}$ erg s is Planck's constant, and $h\nu_1$=13.6 eV is the hydrogen Lyman edge energy. The equivalent Krolik & McKee (1978) ionization parameter (the ratio of the ionizing photon density to the electron density) is $\Gamma \equiv (4\pi/cN_e) \int_{\nu_1}^{\infty} (I_\nu/h\nu) d\nu = 5 \times 10^{-4}$, where we have assumed an 8×10^4 K blackbody radiation field. The He I line ratios are also completely inconsistent with case B values. The large I(He I λ6678)/I(He I λ5876)$\gtrsim 0.5$ ratio typically measured also implies a dense, optically thick nebula (Proga, Mikołajewska, & Kenyon 1994).

Our inference of high optical depth is confirmed by the great strength of O I λ8446 emission. This line can be produced by four mechanisms: recombination, collisional excitation, continuum fluorescence, and Bowen fluorescence by H I Lyβ (Grandi 1980; Rudy et al. 1990). The relative weakness of the O I λ7774 line rules out both recombination and collisional excitation, while the extreme weakness of O I λ7254 and the absence of detectable O I λ7990 rules out continuum fluorescence (Grandi 1980). The only remaining explanation, Bowen fluorescence by Lyβ, operates only in a gas which is optically thick in Hα, yielding

the relation

$$I(\lambda 8446)/I(\mathrm{H}\alpha) = 1.8 \times 10^{-5}/\epsilon_{\mathrm{H}\alpha}, \quad (3)$$

where $\epsilon_{\mathrm{H}\alpha}$ is the escape probability of an Hα photon and a solar O/H abundance ratio is assumed (Grandi 1980). Our measured value of $I(\lambda 8446)/I(\mathrm{H}\alpha)$=0.12 yields $\epsilon_{\mathrm{H}\alpha} = 1.5 \times 10^{-4}$, which corresponds to an optical depth $\tau_{\mathrm{H}\alpha} \sim 4500$ (Ferland & Netzer 1979). This is even higher than the Balmer line estimate above, possibly due to time variability in the optical depth of the region. A prediction of the Bowen fluorescence explanation for the strength of the λ8446 line is that the dereddened photon number fluxes for the O I $\lambda\lambda$1304, 11287 lines should be identical to that of λ8446 (Rudy et al. 1990).

We can use the 1991 August dereddened hydrogen and helium line strengths to estimate the size and structure of the emission-line nebula surrounding the binary. For the H^+ region, using the Hβ emissivity $(4\pi j_{\mathrm{H}\beta}/N_p N_e) = 0.524 \times 10^{-25}$ erg cm^{-3} s^{-1} appropriate for the conditions inferred above from the measured Balmer decrement (Drake & Ulrich 1980), we find the Stromgren radius $R_{\mathrm{H}^+} = 3.7$ AU $D_{10}^{2/3} N_9^{-2/3}$, where D_{10} is the distance to the source in units of 10 kpc and N_9 is the electron density in units of 10^9 cm^{-3}. The emissivity for the He I λ5876 line is $(4\pi j_{5876}/N_{\mathrm{He}^+} N_e) = 0.524 \times 10^{-25}$ erg cm^{-3} s^{-1} for $N_e = 10^{-9}$ cm^{-3} and a 10% helium number abundance, over a wide range of optical depth (Almog & Netzer 1989), from which we estimate $R_{\mathrm{He}^+} = 3.4$ AU $D_{10}^{2/3} N_9^{-2/3}$. Finally, using the case B emissivity for He II λ4686 (Osterbrock 1989), we find $R_{\mathrm{He}^{++}} = 1.3$ AU $D_{10}^{2/3} N_9^{-2/3}$.

We note that the He I ratios showed considerable variability over time. In particular, the two AAT spectra we acquired on 1993 September 10, exposed only 15 minutes apart, show an astonishing difference: the He I $\lambda\lambda$5876, 6678, 7065 and Fe II $\lambda\lambda$6433, 6516 lines, which are clearly detected in the second AAT spectrum (and all of our spectra from other epochs) are completely absent in the first AAT spectrum exposed only 15 minutes earlier! In addition, the He I λ7281 line is 50% weaker in the first spectrum. In all other respects, however, the two spectra are essentially identical (see Figure 6 and Table 8). The variable Fe II $\lambda\lambda$6433, 6516 lines are both from the same multiplet (Moore 1972). The rapid change sets an upper limit of $\lesssim 1.8$ AU on the size of the He^+ region. This is consistent with our calculated Stromgren radius only if $D \lesssim 4 N_9$ kpc. We have no explanation for the rapid change in these line strengths. It cannot be due to the 2-min rotational modulation of the X-ray flux from the neutron star, since both exposures span at least one pulse period. In fact, the longer exposure (in which the line strengths are so low) should have averaged over several pulse periods, in which case we might have expected the lines to be stronger in this exposure.

All of our emission lines indicate a barycentric radial velocity $V \approx -150$ km s^{-1}, consistent with previous measurements (Glass & Feast 1973; Davidsen et al. 1977). Several of our

high-resolution Hα spectra show interesting evolution of the emission line profile (Figure 6). On 1994 Feb 25, the central Hα peak was collapsed, with a peak on the blue wing shifted about 150 km s^{-1} from the line center and an absorption "notch" blue-shifted about 90 km s^{-1} from the line center (left panel of Figure 6). A week later, both the blue-shifted peak and the notch are still present, but the central peak is much stronger (center panel of Figure 6). Four months later, no complex substructure is detected in the line profile (right panel of Figure 6). The 1994 March 7 line profile is comparable to the S-2 type profile identified by van Winckel et al. (1993) in their survey of symbiotic stars, while the 1994 July profile to the S-1 type. These variations may be associated with cyclic changes over the binary orbit (Kenyon 1986). Sood et al. (1995) have proposed to search for orbital-phase modulation of the Hα line profile in order to determine the binary period. The observed line profile variations may be due to orbital-phase variation of the X-ray illumination of the red giant's atmosphere (Schwank, Schmutz, & Nussbaumer 1997).

4. DISCUSSION

4.1. Multiwavelength correlations

Previous authors have cautioned that the association of GX 1+4 and V2116 Oph, although likely, was not completely secure (e.g., Verbunt, Wijers, & Burm 1990). Now, however, the excellent coincidence of the new optical and X-ray astrometry, our evidence for X-ray heating of V2116 Oph during the 1993 September GX 1+4 outburst, and the recent discovery of 2-min optical pulsations from V2116 Oph (Jablonski et al. 1997) all reaffirm the identification of V2116 Oph as the binary companion of GX 1+4. Correlated X-ray/optical intensity behavior is common in LMXBs (e.g., van Paradijs & McClintock 1995), and many investigators have searched for such correlations in GX 1+4.

Throughout the 1970s X-ray bright state of GX 1+4, extremely strong Hα emission was observed from V2116 Oph. During the 1983–1984 X-ray low state established by a series of *EXOSAT* non-detections (Hall & Davelaar 1983; Mukai 1988), Hα emission was present on three occasions but undetected on another (Whitelock et al. 1983; Whitelock 1984; see also Table 4). An examination of Table 6 indicates that several forbidden species ([O III], [Fe VII], [O I]) had substantially stronger line emission during the 1988 July optical observation (contemporaneous with the weak X-ray emission and steady spin-down in GX 1+4; see Makishima et al. 1988). During 1991–1994 (when the X-ray flux was higher), these forbidden features were again weak or even undetected, suggesting that the bright X-ray states may be accompanied by higher electron densities in the symbiotic nebula.

Greenhill et al. (1995) found photometric evidence for a correlated increase in Hα strength during the 1993 September hard X-ray flare, with the optical flare onset leading the X-ray onset by about a month but both ending at roughly the same time. Manchanda et al. (1995) claimed a correlation between spectroscopic Hα strength and hard X-ray flux during 1994 March–June. However, the case for the Manchanda et al. correlation is weak, both due to undersampling of the optical history and because the optical data was correlated against a BATSE pulsed count rate history which was uncorrected for detector viewing angle or detector response.

More recently, an extended X-ray low state beginning in 1996 September (Chakrabarty, Finger, & Prince 1996; Cui & Chakrabarty 1996) was accompanied both by clearly detected Hα emission on October 6 (M. J. Coe 1996, private communication) and an absence of detectable Hα emission on October 16 (Sood et al. 1996). Overall, however, the long-term photometric intensity history of both the Hα feature and the *VRI* bands appears to be correlated with the hard X-ray intensity (Phillips, Greenhill, & Hill 1996). Still, on short time scales, our data indicate that the X-ray activity of the pulsar is an unreliable predictor of the optical and infrared properties of the giant. A comparison of our Hα line strength measurements in Tables 6–8 with simultaneous BATSE measurements of the hard X-ray intensity in Table 1 do not show clear evidence of a correlation. Long-term simultaneous histories of X-ray intensity and Hα emission line strength, if both sampled on sufficiently short time scales, may provide an indirect probe of the accretion disk.

4.2. Source distance and the evolutionary status of the mass donor

Archival X-ray measurements place some constraints on the distance to the system. Following the argument by Chakrabarty et al. (1993), the steady pulsar spin-up rate of $\dot{\nu} \approx 6 \times 10^{-12}$ Hz s^{-1} during the 1970s X-ray bright state (Nagase 1989 and references therein) and its bolometric X-ray flux of 8×10^{-9} erg cm^{-2} s^{-1} (Doty, Hoffman, & Lewin 1981) set a limit of $D \gtrsim 3$ kpc on the distance and $L_x \gtrsim 8 \times 10^{36}$ erg s^{-1} on the X-ray luminosity. We can infer an upper limit of $D \lesssim 15$ kpc by requiring that GX 1+4 not exceed the Eddington critical luminosity ($L_{\rm Edd} = 2 \times 10^{38}$ erg s^{-1}) for spherical accretion onto a neutron star.

The K-band bolometric correction for an M5 III star [for which $(J-K)_0 = 1.23$; Bessell & Brett 1988] is BC$_K = 3.10 \pm 0.05$ (Frogel & Whitford 1987), which (with our measured 1993 June values of $K = 8.13 \pm 0.02$ and $A_K = 0.56 \pm 0.08$) gives an apparent bolometric magnitude of $m_{\rm bol} = 10.67 \pm 0.10$. Combined with the effective temperature $T_{\rm eff} = 3470$ K corresponding to our M5 III spectral classification (Dyck et al. 1996), we

can deduce a distance-radius relation for the red giant: $D = 5.6R_{100}$ kpc, where R_{100} is the radius of the red giant in units of 100 $R_\odot$. Furthermore, the red giant's luminosity must scale as $L_g = 3500D_{10}^2 L_\odot = 1100R_{100}^2 L_\odot$. Similarly, the X-ray luminosity must scale as $L_x = 3 \times 10^{37} R_{100}^2$ erg s^{-1}, roughly consistent with the relation derived from X-ray heating in Section 3.1. The $D \gtrsim 3$ kpc limit from X-ray timing thus implies that $R_g \gtrsim 50R_\odot$ and $L_g \gtrsim 280L_\odot$.

We can use this to further constrain the nature of the companion and the distance to the system. The spectral and luminosity classification of V2116 Oph permits two possibilities for its evolutionary status (see, e.g., Hansen & Kawaler 1994). It may be a low mass star (zero-age main sequence mass $M_{\rm ZAMS} \lesssim 2\,M_\odot$) on the first-ascent red giant branch (FGB), where a degenerate helium core is fed by hydrogen shell burning in the envelope. Alternatively, it may be a low or intermediate mass star ($0.8M_\odot < M_{\rm ZAMS} \lesssim 10M_\odot$) beginning its ascent of the asymptotic giant branch (AGB), where a degenerate carbon-oxygen core is fed by helium and hydrogen shell burning. Statistically speaking, most stars later than M5 III are on the AGB, while most earlier type giants are on the FGB (Judge & Stencel 1991).

The luminosity of both low-mass FGB and AGB stars is almost uniquely determined by the core mass m_c, independent of the mass in their outer envelopes (Joss, Rappaport, & Lewis 1987 and references therein). The maximum luminosity at the tip of the low-mass FGB ($M_{\rm bol} \gtrsim -3.2$) occurs when the degenerate helium core grows large enough ($m_c \approx 0.45M_\odot$) to ignite, leading to an explosive runaway (helium flash) and sending the star onto the horizontal branch. For V2116 Oph, this FGB luminosity limit would imply $D \lesssim 6$ kpc. However, our unheated M6 III classification corresponds to $T_{\rm eff} = 3380 \pm 95$ K, unusually low for an FGB star. Stellar evolution calculations suggest that only a metal-rich star with $M_{\rm ZAMS} \lesssim 2M_\odot$ could have evolved to this temperature before helium flash, and even so must be near the FGB tip (Sweigart, Greggio, & Renzini 1989). If V2116 Oph is on the FGB, it must be close to helium flash, with the following properties: $0.8M_\odot \lesssim M_{\rm ZAMS} \lesssim 2M_\odot$, $280L_\odot \lesssim L_g \lesssim 1300L_\odot$, $50R_\odot \lesssim R_g \lesssim 110R_\odot$, and 3 kpc $\lesssim D \lesssim 6$ kpc. This implies an X-ray luminosity in the range 8×10^{36} erg s$^{-1} \lesssim L_x \lesssim 3 \times 10^{37}$ erg s^{-1} for GX 1+4.

If, on the other hand, V2116 Oph is on the AGB, its spectral classification and the red giant luminosity constraint placed by the X-ray Eddington limit both suggest that it is just beginning it ascent. Without question, the stability of the infrared magnitudes of V2116 Oph (see Table 3) preclude it from being a long-period variable (LPV), since these stars undergo regular $\gtrsim 1$ mag variations in the infrared (Whitelock 1987). LPVs are generally highly evolved AGB stars in which thermal pulsations have set in (Iben & Renzini 1983). By contrast, the X-ray upper limit on the distance strongly constrains V2116 Oph to lie near the bottom of the AGB luminosity range. We can set a *minimum* AGB luminosity by noting

that most AGB stars have $m_c \gtrsim 0.6 M_\odot$, corresponding to $M_{\rm bol} \lesssim -4.7$. Thus, if V2116 Oph is an AGB star, it probably has the following properties: $0.8 M_\odot \lesssim M_{\rm ZAMS} \lesssim 10 M_\odot$, $4800 L_\odot \lesssim L_g \lesssim 8000 L_\odot$, $210 R_\odot \lesssim R_g \lesssim 270 R_\odot$, and 12 kpc $\lesssim D \lesssim$ 15 kpc. This implies an X-ray luminosity in the range 1×10^{38} erg s$^{-1} \lesssim L_x \lesssim 2 \times 10^{38}$ erg s^{-1} for GX 1+4.

The two different possibilities for which giant branch V2116 Oph is ascending lead to two distinct distance ranges, and it is not obvious which possibility is more likely. Unfortunately, there is no straightforward way to observationally distinguish the FGB and AGB for M giant stars (Judge & Stencel 1991). Statistically, an intrinsically M6 III star is somewhat likelier to be on the AGB. In the case of an FGB star, our lower luminosity limit $L_g \gtrsim 280 L_\odot$ implies a core mass $m_c \gtrsim 0.34 M_\odot$ (Joss et al. 1987), which places the star close enough (within $\sim 10^7$ yr) to helium flash to make finding it there somewhat unlikely. However, the measured interstellar extinction to V2116 Oph ($A_V \approx 5$) is rather low for the $\gtrsim 10$ kpc line of sight through the Galactic plane which is required if the star is on the AGB, while it is quite reasonable for a closer ($\lesssim 6$ kpc) distance (e.g., Spitzer 1978). Also, a distance of $\lesssim 4$ kpc is apparently required to reconcile the Stromgren radius of the He^+ region with the size implied by the rapid line variability we observed in 1993 September, which is inconsistent with the AGB solution. We therefore consider it most likely that V2116 Oph is on the FGB at a distance of 3–6 kpc. A summary of our conclusions is given in Table 9.

4.3. The accretion disk

Since optical emission line diagnostics suggest that the symbiotic nebula enshrouding the binary is powered by ultraviolet radiation rather than the neutron star's X-ray emission (Section 3.3), we conclude that an accretion disk is present in the system. The recent discovery of 2-min coherent optical pulsations at short wavelengths (Jablonski et al. 1997) is probably a sign of X-ray reprocessing in this accretion disk (Chester 1979). Our emission line observations provide a crude measure of the shape of the disk's ultraviolet continuum spectrum through the Iijima K-parameter, defined as the number of He^+-ionizing photons relative to the H^0-ionizing and He^0-ionizing photons. This parameter can be computed using optical emission line strengths (Iijima 1981),

$$K = \frac{\int_{4\nu_1}^{\infty} (L_\nu / h\nu) d\nu}{\int_{\nu_1}^{4\nu_1} (L_\nu / h\nu) d\nu} = \frac{2.2\, I({\rm He\ II}\ \lambda 4686)}{4.16\, I({\rm H}\beta) + 9.94\, I({\rm He\ I}\ \lambda 4471)}, \tag{4}$$

where L_ν is the overall disk luminosity at frequency ν, and $h\nu_1 = 13.6$ eV. Our 1991 August line strengths yield $K = 0.03$. We note that this value is actually an upper limit, since Hβ strength may be depressed by optical depth effects (Kenyon 1986).

The overall luminosity from a geometrically thin, optically thick accretion disk is given by

$$L_\nu \approx \frac{16\pi^2 h\nu^3}{c^2} \int_{r_{\rm in}}^{r_{\rm out}} \frac{r\,dr}{\exp[h\nu/kT(r)] - 1}, \tag{5}$$

where $k = 1.4 \times 10^{-16}$ erg K^{-1} is Boltzmann's constant, c is the velocity of light, $r_{\rm in}$ and $r_{\rm out}$ are the inner and outer radii of the disk, and $T(r)$ is the disk's temperature profile as a function of mid-plane radius r. For an X-ray heated disk, we may consider the disk as consisting of up to three distinct regions: an innermost region powered primarily by internal viscous dissipation, a middle region of "shallow" X-ray heating, and an outer region of "deep" X-ray heating (e.g., Cunningham 1976; Arons & King 1993). We consider each of these regions in turn.

The standard temperature profile for an unirradiated thin accretion disk is set by internal viscous dissipation (Shakura & Sunyaev 1973; Frank, King, & Raine 1992)

$$T_0 = \left(\frac{3GM_x\dot{M}}{8\pi\sigma r^3}\right)^{1/4} = 1.3 \times 10^4\ M_{1.4}^{1/4}\,\dot{M}_{-9}^{1/4}\,r_{10}^{-3/4}\ \ {\rm K}, \tag{6}$$

where $M_{1.4}$ is the neutron star mass M_x in units of 1.4 $M_\odot$, $\dot{M}_{-9}$ is the mass accretion rate $\dot{M}$ in units of 10^{-9} $M_\odot$ yr^{-1}, and r_{10} is the mid-plane radius in units of 10^{10} cm. At sufficiently small radii, this internal heating will dominate over X-ray heating in setting the disk temperature. Beyond a critical radius, however, X-ray heating of the disk surface will modify the temperature profile according to

$$T_{\rm irr} = (T_0^4 + T_x^4)^{1/4}. \tag{7}$$

If we assume that the disk is irradiated by a central X-ray point source, then we can write T_x as

$$T_x = \left[\frac{L_x(1-\eta_d)}{4\pi\sigma r^2}\cos\psi\right]^{1/4} \approx \left[\frac{L_x(1-\eta_d)}{4\pi\sigma r^2}\left(\frac{dH}{dr} - \frac{H}{r}\right)\right]^{1/4}, \tag{8}$$

where η_d is the X-ray albedo of the disk, ψ is the angle between the normal to the disk surface and the vector from the neutron star, and H is the disk's scale height. Thus, we see that the temperature profile due to X-ray heating is sensitive to the functional form of $H(r)$ through the approximation for $\cos\psi$ (which assumes $H \ll r$).

In the shallow X-ray heating region, the surface temperature profile is set by X-ray heating but the *central* temperature of the disk is still set by internal viscous dissipation. Thus, the disk thickness has the usual value for a standard unirradiated thin disk (Shakura & Sunyaev 1973; Frank et al. 1992),

$$H = 1.7 \times 10^8\ \alpha^{-1/10}\,M_{1.4}^{-3/8}\,\dot{M}_{-9}^{3/20}\,r_{10}^{9/8}\ {\rm cm}, \tag{9}$$

where α is an order unity dimensionless parameterization of the kinematic viscosity $\nu_{\rm visc} = \alpha c_s H$, and c_s is the isothermal sound speed. We thus find

$$T_x = 2.3 \times 10^4 \ \alpha^{-1/40} \, (1-\eta_d)^{1/4} \, M_{1.4}^{5/32} \, \dot{M}_{-9}^{23/80} \, r_{10}^{-15/32} \ {\rm K}. \tag{10}$$

Shallow X-ray heating will dominate internal viscous heating in setting the disk surface temperature at radii exceeding roughly 10^9 cm.

If $T_x^4 \gtrsim \tau T_0^4$, then X-ray heating will also dominate internal heating in setting the *central* temperature of the disk (Lyutyi & Sunyaev 1976; Spruit 1995). Here, τ is the disk's optical depth, given by $\tau = 54 \, \alpha^{-4/5} \, \dot{M}_{-9}^{1/5}$ for a standard α-disk (Frank et al. 1992). In this region of deep X-ray heating, the vertical structure of the disk will not obey the $H \propto r^{9/8}$ relationship in equation (9), but will instead follow a $H \propto r^{9/7}$ power law (e.g., Cunningham 1976; Vrtilek et al. 1990; Arons & King 1993). Deep X-ray heating "puffs up" the outer disk so that

$$H = 1.1 \times 10^9 \ (1-\eta_d)^{1/7} \, M_{1.4}^{-3/7} \, \dot{M}_{-9}^{1/7} \, r_{10}^{9/7} \ {\rm cm}, \tag{11}$$

from which we find

$$T_x = 2.7 \times 10^4 \ (1-\eta_d)^{2/7} \, M_{1.4}^{1/7} \, \dot{M}_{-9}^{2/7} \, r_{10}^{-3/7} \ {\rm K}. \tag{12}$$

Deep X-ray heating will dominate over shallow heating at radii exceeding roughly 2×10^{10} cm.

With the appropriate choice of temperature profile, equations (4) and (5) can be used to predict the Iijima K-parameter that should be measured due to photoionzation by the disk's continuum emission. The most important parameter for determining K will be the inner disk radius $r_{\rm in}$. For an X-ray pulsar, $r_{\rm in}$ should be roughly equal to the magnetospheric radius r_m, where the neutron star magnetosphere disrupts the Keplerian disk flow (e.g. Frank et al. 1992)

$$r_{\rm in} = r_m = 3 \times 10^8 \ {\rm cm} \ \left(\frac{L_x}{10^{37} \ {\rm erg \ s^{-1}}} \right)^{-2/7} \left(\frac{B}{10^{12} \ {\rm G}} \right)^{4/7}, \tag{13}$$

where B is the surface dipole magnetic field of the neutron star. If GX 1+4 has a magnetic field strength typical of X-ray pulsars ($B \sim 10^{12}$ G), then we expect $r_{\rm in} \approx 3 \times 10^8$ cm. In this case, there will be a hot inner region of the disk which is primarily powered internal viscous dissipation. Most of the photons capable of ionizing He^+ will come from this region.

However, GX 1+4 has undergone several torque reversals between steady spin-up and spin-down of the pulsar (Makishima et al. 1988; Chakrabarty et al. 1997). Standard accretion torque theory (e.g., Ghosh & Lamb 1979) would therefore predict that the pulsar is spinning near its equilibrium spin period, which occurs when r_m (and thus $r_{\rm in}$) is close

to the corotation radius $r_{\rm co} = (GM_x P_{\rm spin}^2/4\pi^2)^{1/3}$,where the magnetic field lines move at the local Kepler velocity. For a slow rotator like GX 1+4, the corotation radius is very large ($r_{\rm co} \approx 3 \times 10^9$ cm). An ultrastrong pulsar magnetic field ($B \sim 10^{14}$ G) would be required to disrupt the disk at such a large distance from the neutron star. The innermost region of this disk would be dominated by shallow X-ray heating, and would be much cooler than the inner edge of a disk terminating at 3×10^8 cm; the expected He II λ4686 line strength would be correspondingly weaker. Since these two values of $r_{\rm in}$ will result in significantly different temperature profiles for the disk, it is interesting to compare the predicted values of K in each case with the value we measure.

We have modeled the accretion disk in GX 1+4 as a standard thin disk irradiated by a central X-ray source, as described above. To provide for a smooth transition between the different heating regimes in a simple way, we have used the sum of equations (9) and (11) for the disk thickness and calculated the temperature profile according to equations (6), (7), and (8). We assume the disk cuts off sharply at an outer boundary set by the tidal radius of the neutron star ($\approx 0.9 R_{\rm Roche} \sim 10^{13}$ cm; Frank et al. 1992). We consider two cases: that of an FGB donor and an X-ray luminosity of $L_x \approx 10^{37}$ erg s^{-1}, and that of an AGB donor and $L_x \approx 10^{38}$ erg s^{-1}. In each case, we consider a wide range of pulsar magnetic field strengths ranging from $B \sim 10^{12}$ G ("weak") to $B \sim 10^{14}$ G ("strong"), and compute the inner disk radius according to equation (13). Finally, in integrating the numerator of equation (4), we cut off the disk spectrum above 1 keV, since the photoionization rate is already negligible at this energy. Our calculations are not sensitive to the exact choice of either this upper bound or $r_{\rm out}$. We assumed that the disk had an effective X-ray albedo $\eta_d = 0.9$ (de Jong, van Paradijs, & Augusteijn 1996).

The resulting values for K are plotted in Figure 7. We see immediately that given a measured K, the type of mass donor (and thus the X-ray luminosity) strongly constrains the magnetic field strength and thus the inner disk radius. Specifically, if the mass donor is an FGB star, then the pulsar *cannot* be near its equilibrium spin period; instead, the accretion disk must terminate well inside $r_{\rm co}$ in order to produce enough hard UV photons to produce the observed He II λ4686 strength. In this case, a surface dipole magnetic field strength of $\sim 5 \times 10^{12}$ G is expected for the pulsar. On the other hand, if the mass donor is an AGB star, then the pulsar magnetic field *must* be ultrastrong ($\sim 10^{14}$ G) in order to terminate the disk at a relatively large radius; otherwise, a considerably stronger He II line ought to have been observed. This would be consistent with the pulsar spinning close to its equilibrium spin period. Although these results are based on a rather simple model for the accretion disk and the photoionized nebula, our qualitative conclusions should be quite secure.

Since we regard it as rather more likely that the mass donor is an FGB star, this

analysis raises important doubts about the applicability of standard accretion torque theory in explaining the observed pulsar torque reversals in GX 1+4.

4.4. Limits on the orbital period

Given a neutron star mass $M_x = 1.4\,M_\odot$ and a maximum mass and minimum radius for the red giant, we can compute a lower limit on the orbital period (independent of the mass transfer mode) by requiring that the giant fit inside its Roche lobe. The size of the Roche lobe is $(R_L/a) \approx 0.49q^{2/3}[0.6q^{2/3} + \ln(1 + q^{1/3})]^{-1}$, where R_L is the radius of a sphere with the same volume as the giant's Roche lobe, a is the binary separation, and $q = M_g/M_x$ is the mass ratio of the red giant and the neutron star (Eggleton 1983). For the FGB case, we have $M_g \lesssim 2M_\odot$ and $R_g \gtrsim 50R_\odot$, implying that $P_{\rm orb} \gtrsim 100$ d. (Because of its low effective temperature, V2116 Oph is likeliest to be very close to helium flash in the FGB case, where $R_g \approx 100R_\odot$. This would imply $P_{\rm orb} \gtrsim 280$ d.) For the AGB case, $M_g \lesssim 10M_\odot$ and $R_g \gtrsim 210R_\odot$, implying that $P_{\rm orb} \gtrsim 260$ d. Overall, we see that the binary period for the system is probably of order a year or more, by far the longest of any known LMXB. These conclusions are included in Table 9.

If we assume that the mass transfer onto the neutron star is driven by Roche lobe overflow, then we can use a similar argument to estimate an upper limit on the orbital period by taking the minimum mass and maximum radius of the giant and requiring that it fill its Roche lobe. If we neglect mass loss, then $M_g \gtrsim 0.8M_\odot$ for both the FGB and AGB cases. In the FGB case, $R_g \lesssim 110R_\odot$ and so $P_{\rm orb} \lesssim 480$ d, while in the AGB case $R_g \lesssim 270R_\odot$ and $P_{\rm orb} \lesssim 5$ yr. With mass loss, we have $M_g \gtrsim 0.34M_\odot$ for the FGB and $M \gtrsim 0.6M_\odot$ for the AGB, yielding $P_{\rm orb} \lesssim 2$ yr and $P_{\rm orb} \lesssim 6$ yr, respectively. However, we emphasize that these upper limits on the size of the binary are only meaningful if the giant fills its Roche lobe.

Due to the large variations in the accretion torque on GX 1+4 on ∼100 d time scales, detection of orbital variations in the X-ray pulse timing data has proven elusive (Chakrabarty et al. 1997). Cutler, Dennis, & Dolan (1986) suggested a 304 d binary period based on an examination of the 1970s accretion torque history of GX 1+4, but this remains unconfirmed and may be an artifact of the strong $1/f$ torque noise in the pulsar's spin behavior (Bildsten et al. 1997). Sood et al. (1995) have proposed to measure the orbital period by searching for cyclic variations in the Hα emission line profile, a promising technique given the strength of the line feature. Another possible approach would be to look for a low amplitude cycle in the infrared magnitudes due to orbit-modulated X-ray heating. For heating by a steady X-ray source, the peak-to-peak fractional change in the red giant's luminosity should be

$(\Delta L_g/L_g) \lesssim 1 - (T_{\rm cool}/T_{\rm hot})^4$, with the exact amplitude depending upon the binary inclination angle. Taking $T_{\rm cool} = 3370$ K and $T_{\rm hot} = 3470$ K, we expect infrared variations of $\Delta K \lesssim 0.1$ mag. The scatter in the current infrared photometric data is ~ 0.2 mag (see Table 3), but more precise measurements are feasible. In addition, a precise radial velocity curve for the red giant should be measurable using the infrared CO absorption bands near 2.3 μm. Since V2116 Oph is quite bright in this band ($K \approx 8$), it is an excellent candidate for such measurements.

4.5. Mass loss from the red giant and binary mass transfer

We first consider the possibility that mass donor fills its Roche lobe. A donor mass of $M_g \lesssim 1 M_\odot$ is required to avoid dynamically unstable mass transfer, and even then the mass transfer rate in a binary as wide as GX 1+4 must be highly super-Eddington (Kalogera & Webbink 1996), with a value of $\sim 10^{-7} M_\odot$ yr^{-1} for an FGB star (Webbink et al. 1983) and $\sim 10^{-6}$ for an AGB star (de Kool, van den Heuvel, & Rappaport 1986). Since Roche lobe overflow would thus imply prodigious mass loss from the binary, an earlier suggestion of radio jets from GX 1+4 (Manchanda 1993) is intriguing. However, more sensitive radio observations indicate that the proposed jets are probably field sources unassociated with GX 1+4 (Fender et al. 1997; Marti et al. 1997). Further searches for evidence of a strong outflow from GX 1+4 would be of great interest.

Steady accretion in LMXBs with Roche-lobe-filling evolved donors should be rare due to dwarf-nova-like instabilities in the accretion disk (King, Kolb, & Burderi 1996). A binary as wide as GX 1+4 will undergo stable mass transfer only for the short time that the red giant mass remains $\gtrsim 0.9 M_\odot$, and will spend the remainder of its X-ray-emitting lifetime (i.e. until the red giant envelope is exhausted or ejected) as a soft X-ray transient (King et al. 1997b). Systems whose donor envelope is still sufficiently massive to avoid the disk instability must still somehow shield the donor from X-ray irradiation, possibly with an accretion disk corona, in order to avoid violent thermally-unstable mass transfer (King et al. 1997a). Since GX 1+4 is a persistent X-ray source, must be in a very short-lived ($\lesssim 10^6$ yr) stable accretion state if powered by Roche-lobe-overflow, and it will soon become a soft X-ray transient.

An alternative scenario is that the V2116 Oph does not fill its Roche lobe, but that the accretion disk around GX 1+4 forms from the wind of the red giant. This scenario is particularly attractive in the context of explaining the accretion torque behavior of the pulsar. Chakrabarty et al. (1997) found that the torque on the pulsar is anticorrelated with the hard X-ray luminosity (which is presumably proportional to $\dot{M}$), the opposite of what

is predicted by standard accretion torque theory (Ghosh & Lamb 1979). To explain these observations, Nelson et al. (1997) have revived earlier suggestions (Makishima et al. 1988; Dotani et al. 1989) that the spin-down may be due to episodic formation of a retrograde accretion disk, with disk material rotating with the opposite sense as the pulsar. Although such a scenario is difficult to understand if the mass donor fills its Roche lobe, it seems plausible if the disk were formed from the slow, dense wind of the red giant. In this case, the unusually strong surface magnetic field invoked by standard accretion torque theory (see Section 4.3) is not required, since the pulsar need not be near its equilibrium spin period. This also fits nicely with two other inferences we made previously: that the mass donor is probably an FGB star (Section 4.2), and that the pulsar is probably not near its equilibrium spin period if the donor is an FGB star (Section 4.3).

However, it is not clear that wind accretion can provide a sufficiently high $\dot{M}$ in this system. In typical symbiotic binaries, ionization of the red giant wind by the hot component results in radio continuum emission due to thermal bremsstrahlung, whose intensity can be related to the giant's mass loss rate $\dot{M}_w$ (Seaquist & Taylor 1990). A marginal detection of radio emission from the GX 1+4/V2116 Oph system (0.06 ± 0.02 mJy at 6 cm; Marti et al. 1997) establishes the scale for the mass loss rate through a stellar wind of

$$-\dot{M}_w \approx 1 \times 10^{-7} M_\odot \, \mathrm{yr}^{-1} \left(\frac{v_w}{10 \text{ km s}^{-1}} \right) \left(\frac{D}{10 \text{ kpc}} \right)^{3/2} \left(\frac{S_{6\mathrm{cm}}}{0.06 \text{ mJy}} \right)^{3/4}, \qquad (14)$$

where v_w is the wind velocity and we have used the mass-loss formula of Wright & Barlow (1975). Naively assuming a spherically symmetric wind, this mass loss rate is roughly consistent with that expected for $v_w = 10$ km s^{-1}, given the inferred electron density ($N_e \sim 10^9$ cm^{-3}) and scale size ($R \sim 10^{13}$ cm) of the photoionized nebula enshrouding the binary. However, such a small mass-loss rate cannot power a 10^{38} erg s^{-1} X-ray source, and an unusually high accretion efficiency would be required to power even a 10^{37} erg s^{-1} source for the ~ 10 km s^{-1} wind velocity typically expected from red giants.

On the other hand, most of what is known about M giant wind velocities is based on observations of late AGB stars; the winds from FGB or early AGB stars might be somewhat faster, allowing a higher mass loss rate in Equation (10). Indeed, there is preliminary evidence for a ≈ 100 km s^{-1} outflow from V2116 Oph (Chakrabarty, van Kerkwijk, & Larkin 1997, in preparation). Thus, wind accretion remains a viable possibility, at least for a sub-Eddington X-ray source. Even if the pulsar is currently wind-fed, nuclear evolution of the red giant may still eventually lead to Roche lobe overflow.

This paper was based in part on observations at Palomar Observatory, which is owned and operated by the California Institute of Technology. D.C. thanks Tom Prince and Fiona

Harrison for acting as faculty sponsors for the Palomar and *ROSAT* investigations during his graduate work at Caltech. We are grateful to Lee Armus, Colin Aspin, Dave Buckley, Robert Knop, Stuart Lumsden, and Jesper Storm for generously obtaining service observations for us, and to Malcolm Coe, Juan Fabregat, Jules Halpern, and Shri Kulkarni for sharing archival data with us. We thank Mike Read for providing astrometric measurements of the UK Schmidt plate, and Hannah Quaintrell, Luisa Morales, and Lucie Green for assistance in reducing the optical data. It is a pleasure to acknowledge Lars Bildsten, Malcolm Coe, Marshall Cohen, Rob Fender, Bob Hill, Scott Kenyon, Davy Kirkpatrick, Rob Nelson, Gerry Neugebauer, Angela Putney, Saul Rappaport, Ian Thompson, and John Wang for helpful discussions and advice. An anonymous referee made several useful suggestions.

This work was supported in part by NASA grant NAG 5-2956 under the *ROSAT* Guest Observer program. D.C. was supported by a NASA GSRP Graduate Fellowship at Caltech under grant NGT-51184 and by a NASA Compton Postdoctoral Fellowship at MIT under grant NAG 5-3109. P.R. thanks the Nuffield Foundation for financial support for himself and L. Green.

REFERENCES

Allen, D. A. 1980, MNRAS, 190, 75

Allen, D. A. 1982, in The Nature of Symbiotic Stars, ed. M. Friedjung & R. Viotti (Dordrecht: Reidel), 27

Almog, Y. & Netzer, H. 1989, MNRAS, 238, 57

Arons, J. & King, I. R. 1996, ApJ, 413, L121

Baker, J. G. & Menzel, D. H. 1938, ApJ, 88, 52

Baldwin, J. A., Phillips, M. M., & Terlevich, R. 1981, PASP, 93, 5

Becker, R. H., Boldt, E. A., Holt, S. S., Pravdo, S. H., Rothschild, R. E., Selemitsos, P. J., & Swank, J. H. 1976, ApJ, 207, L167

Bessell, M. S. & Brett, J. M. 1988, PASP, 100, 1134

Bildsten, L. et al. 1997, ApJS, accepted for publication

Camilo, F. 1995, Ph.D. thesis, Princeton University

Chakrabarty, D. 1996, Ph.D. thesis, California Institute of Technology

Chakrabarty, D. et al. 1993, ApJ, 403, L33

Chakrabarty, D. et al. 1994, in Second Compton Symposium, ed. C. E. Fichtel, N. Gehrels, & J. P. Norris, (New York: AIP Press), 390

Chakrabarty, D. et al. 1997, ApJ, 481, L101

Chakrabarty, D., Finger, M. H., & Prince, T. A. 1996, IAU Circ., No. 6478

Chester, T. J. 1979, ApJ, 227, 569

Cui, W. & Chakrabarty, D. 1996, IAU Circ., No. 6478
Cunningham, C. 1976, ApJ, 208, 534
Cutler, E. P., Dennis, B. R., & Dolan, J. F. 1986, ApJ, 300, 551
Davidsen, A., Malina, R., & Bowyer, S. 1977, ApJ, 211, 866
de Jong, J. A., van Paradijs, J., & Augusteijn, T. 1996, A&A, 314, 484
de Kool, M., van den Heuvel, E. P. J., & Rappaport, S. A. 1986, A&A, 164, 73
Dotani, T., Kii, T., Nagase, F., Makishima, K., Ohashi, T., Sakao, T., Koyama, K., & Tuohy, I. R. 1989, PASJ, 41, 427
Doty, J. P., Hoffman, J. A., & Lewin, W. H. G. 1981, ApJ, 243, 257
Doxsey, R., Apparao, K. M. V., Bradt, H. V., Dower, R. G., & Jernigan, J. G. 1977, Nature, 270, 586
Doyon, R., Joseph, R. D., & Wright, G. S. 1994, ApJ, 421, 101
Drake, S. A. & Ulrich, R. K. 1980, ApJS, 42, 351
Dyck, H. M., Benson, J. A., van Belle, G. T., & Ridgway, S. T. 1996, AJ, 111, 1705
Eggleton, P. P. 1983, ApJ, 268, 368
Fender, R. P., Roche, P. D., Pooley, G. G., Chakrabarty, D., Tzioumis, A. T., & Spencer, R. E. 1997, in The Transparent Universe, ed. C. Winkler, T. J. L. Courvoisier, & P. Durouchoux (Noordwijk: ESA SP-382), 303
Ferland, G. & Netzer, H. 1979, ApJ, 229, 274
Finger, M. H., Koh, D. T., Nelson, R. W., Prince, T. A., Vaughan, B. A., & Wilson, R. B. 1996, Nature, 381, 291
Frank, J., King, A., & Raine, D. 1992, Accretion Power in Astrophysics, 2nd ed. (Cambridge: Cambridge U. Press)
Frogel, J. A. & Whitford, A. E. 1987, ApJ, 320, 199
Garcia, M. et al. 1983, ApJ, 267, 291
Ghosh, P. & Lamb, F. K. 1979, ApJ, 234, 296
Glass, I. S. 1979, MNRAS, 187, 807
Glass, I. S. & Feast, M. W. 1973, Nature Phys. Sci., 245, 39
Gorenstein, P. 1975, ApJ, 198, 95
Gotthelf, E., Halpern, J., & Szentgyorgyi, A. 1988, IAU Circ., No. 4635
Graham, J. R., Matthews, K., Greenstein, J. L., Neugebauer, G., Tinney, C. G., & Persson, S. E. 1992, AJ, 104, 2016
Grandi, S. A. 1980, ApJ, 238, 10
Greenhill, J. G., Watson, R. D., Tobin, W., Pritchard, J. D., & Clark, M. 1995, MNRAS, 274, L59
Hall, R. & Davelaar, J. 1983, IAU Circ., No. 3872
Hansen, C. J. & Kawaler, S. D. 1994, Stellar Interiors: Physical Principles, Structure, and Evolution (New York: Springer-Verlag)

Iben, I. & Renzini, A. 1983, ARA&A, 21, 271

Iben, I. & Tutukov, A. V. 1996, ApJS, 105, 145

Iijima, T. 1981, in Photometric and Spectroscopic Binary Systems, ed. E. B. Carling & Z. Kopal (Dordrecht: Reidel), 517

Jablonski, F. J., Pereira, M. G., Braga, J., & Gneiding, C. D. 1997, ApJ, 482, L171

Joss, P. C., Rappaport, S., & Lewis, W. 1987, ApJ, 319, 180

Judge, P. G. & Stencel, R. E. 1991, ApJ, 371, 357

Kalogera, V. & Webbink, R. F. 1996, ApJ, 458, 301

Kenyon, S. J. 1986, The Symbiotic Stars, (Cambridge: Cambridge Univ. Press)

Kenyon, S. J. & Fernandez-Castro, T. 1987, AJ, 93, 938

King, A. R., Frank, J., Kolb, U., & Ritter, H. 1997a, ApJ, 482, 919

King, A. R., Frank, J., Kolb, U., & Ritter, H. 1997b, ApJ, 484, in press

King, A. R., Kolb, U., & Burderi, L. 1996, ApJ, 464, L127

Kirkpatrick, J. D., Henry, T. J., & McCarthy, D. W. 1991, ApJS, 77, 417

Kleimann, S. G. & Hall, D. N. B. 1986, ApJS, 62, 501

Krolik, J. H. & McKee, C. F. 1978, ApJS, 37, 459

Lewin, W. H. G., Ricker, G. R., & McClintock, J. E. 1971, ApJ, 169, L17

Lyutyi, V. M. & Sunyaev, R. A. 1976, Sov. Astron., 20, 290

Makishima, K. et al. 1988, Nature, 333, 746

Manchanda, R. K. 1993, Adv. Space Res., 13(12), 331

Manchanda, R. K., James, S. D., Lawson, W. A., Sood, R. K., Grey, D. J., & Sharma, D. P. 1995, A&A, 293, L29

Marti, J., Mirabel, I. F., Chaty, S., & Rodriguez, L. F. 1997, in The Transparent Universe, ed. C. Winkler, T. J. L. Courvoisier, & P. Durouchoux (Noordwijk: ESA SP-382), 323

Meinel, A. B., Aveni, A. F., & Stockton, M. W. 1975, Catalog of Emission Lines in Astrophysical Objects, 2nd ed., University of Arizona Optical Sciences Center Technical Report 27

Moore, C. E. 1972, Multiplet Table of Astrophysical Interest (National Bureau of Standards–National Standard Reference Data Series, No. 40)

Mukai, K. 1988, The 1988 Low State of GX 1+4, Mullard Space Science Laboratory internal report

Munari, U., Yudin, B. F., Taranova, O. G., Massone, G., Marang, F., Roberts, G., Winkler, H., & Whitelock, P. A. 1992, A&AS, 93, 383

Nagase, F. 1989, PASJ, 41, 1

Nelson, R. W. et al. 1997, in Accretion Phenomena and Associated Outflows, ed. D. Wickramasinghe, L. Ferrario, & G. Bicknell (San Francisco: Astron. Soc. of the Pacific), in press

Osterbrock, D. E. 1989, Astrophysics of Gaseous Nebulae and Active Galactic Nuclei (Mill Valley, CA: University Science)

Phillips, J., Greenhill, J., & Hill, K. M. 1996, IAU Circ., No. 6528

Phinney, E. S. & Kulkarni, S. R. 1994, ARA&A, 32, 591

Predehl, P., Friedrich, S., & Staubert, R. 1994, A&A, 294, L33

Proga, D., Kenyon, S. J., Raymond, J. C., & Mikołajewska, J. 1996, ApJ, 471, 930

Proga, D., Mikołajewska, J., & Kenyon, S. J. 1994, MNRAS, 268, 213

Ridgway, S. T., Joyce, R. R., White, N. M., & Wing, R. F. 1980, ApJ, 235, 126

Rieke, G. H. & Lebofsky, M. J. 1985, ApJ, 288, 618

Rudy, R. J., Cohen, R. D., Rossano, G. S., & Puetter, R. C. 1990, ApJ, 362, 346

Schmid, H. M. 1989, A&A, 211, L31

Schwank, M., Schmutz, W., & Nussbaumer, H. 1997, A&A, 319, 166

Seaquist, E. R. & Taylor, A. R. 1990, ApJ, 349, 313

Shahbaz, T., Smale, A. P., Naylor, T., Charles, P. A., van Paradijs, J., Hassall, B. J. M., & Callanan, P. 1996, MNRAS, 282, 1437

Shakura, N. I. & Sunyaev, R. A. 1973, A&A, 24, 337

Sharma, D. P., Sood, R. K., Stringfellow, G., James, S. D., Hill, K. M., & Manchanda, R. K. 1993, Adv. Space. Res., 13(12), 375

Shortridge, K. 1991, Figaro: General Data Reduction and Analysis (UK Starlink User Document)

Sood, R. K. et al. 1991, IAU Circ., No. 5381

Sood, R. K., James, S. D., Lawson, W. A., Sharma, D. P., Grey, D. G., & Manchanda, R. K. 1995, Adv. Space Res., 16(3), 131

Sood, R., James, S., Lawson, W. & Manchanda, R. K. 1996, IAU Circ., No. 6496

Spitzer, L. 1978, Physical Processes in the Interstellar Medium (New York: Wiley)

Spruit, H. C. 1995, in The Lives of the Neutron Stars, ed. M. A. Alpar, U. Kiziloglu, & J. van Paradijs (Dordrecht: Kluwer)

Sweigart, A. V., Greggio, L., & Renzini, A. 1989, ApJS, 69, 911

Taam, R. E. & van den Heuvel, E. P. J. 1986, ApJ, 305, 235

Terndrup, D. M., Frogel, J. A., & Whitford, A. E. 1990, ApJ, 357, 453

Tsuji, T. 1966, PASJ, 18, 127

van Paradijs, J. 1996, ApJ, 464, L139

van Paradijs, J. & McClintock, J. E. 1995, in X-Ray Binaries, ed. W. H. G. Lewin, J. van Paradijs, & E. P. J. van den Heuvel (Cambridge: Cambridge U. Press), 58

van Winckel, H., Duerbeck, H. W., & Schwarz, H. E. 1993, A&AS, 102, 401

Veilleux, S. & Osterbrock. D. E. 1987, ApJS, 63, 295

Verbunt, F. & van den Heuvel, E. P. J. 1995, in X-Ray Binaries, ed. W. H. G. Lewin, J. van Paradijs, & E. P. J. van den Heuvel (Cambridge: Cambridge U. Press), 457

Verbunt, F., Wijers, R. A. M. J., & Burm, H. M. G 1990, A&A, 234, 195
Vrtilek, S. D., Raymond, J. C., Garcia, M. R., Verbunt, F., & Hasinger, G. 1990, A&A, 235, 162
Webbink, R. F., Rappaport, S., & Savonije, G. J. 1983, ApJ, 270, 678
Webster, B. L. & Allen, D. A. 1975, MNRAS, 171, 171
Whelan, J. A. J. et al. 1977, MNRAS, 181, 259
Whitelock, P. A. 1984, IAU Circ., No. 3919
Whitelock, P. A. 1987, PASP, 99, 573
Whitelock, P. A., Menzies, J. W., & Feast, M. W. 1983, IAU Circ., No. 3885
Wing, R. F. 1981, in Physical Processes in Red Giants, ed. I. Iben & A. Renzini (Dordrecht: Reidel), 41
Wright, A. E., & Barlow, M. J. 1975, MNRAS, 170, 41

Table 1. Pulsed Hard X-ray Intensity of GX 1+4

Date	20–60 keV Pulsed Flux[a]
1991 Jul 01	33 ± 3
1991 Aug 10	36 ± 4
1993 Apr 06	13 ± 2
1993 Jun 25	29 ± 3
1993 Jun 30	44 ± 3
1993 Jul 05	31 ± 5
1993 Sep 08	124 ± 3
1994 Feb 25	8 ± 4
1994 Mar 07	15 ± 3
1994 Jun 30	15 ± 4
1995 Mar 12	75 ± 4
1995 Aug 14	41 ± 4
1996 Mar 26	103 ± 5

[a]In units of 10^{-11} erg cm^{-2} s^{-1}.

Table 2. Optical Astrometry and Photometry of the GX 1+4 Field[a]

Star[b]	RA (J2000)	Dec. (J2000)	B	V	R
V2116 Oph	$17^h\,32^m\,02\overset{s}{.}06$	$-24^\circ\,44'\,45\overset{''}{.}5$	20.78(5)	18.40(3)	15.99(1)
NNE	$17^h\,32^m\,02\overset{s}{.}12$	$-24^\circ\,44'\,39\overset{''}{.}5$	> 23	21.0(3)	19.54(8)
2	$17^h\,32^m\,03\overset{s}{.}59$	$-24^\circ\,44'\,24\overset{''}{.}6$	20.62(5)	18.57(4)	16.60(2)
3	$17^h\,32^m\,03\overset{s}{.}13$	$-24^\circ\,44'\,30\overset{''}{.}2$	22.6(2)	19.39(7)	17.48(2)
4	$17^h\,32^m\,03\overset{s}{.}05$	$-24^\circ\,44'\,40\overset{''}{.}3$	22.6(2)	19.7(1)	18.24(4)
6	$17^h\,32^m\,03\overset{s}{.}36$	$-24^\circ\,44'\,53\overset{''}{.}9$	22.2(2)	18.75(4)	16.82(1)
9	$17^h\,32^m\,03\overset{s}{.}76$	$-24^\circ\,45'\,33\overset{''}{.}8$	14.76(1)	13.13(1)	< 12.8
10	$17^h\,32^m\,00\overset{s}{.}37$	$-24^\circ\,44'\,06\overset{''}{.}5$	17.28(1)	15.66(1)	15.05(1)
12	$17^h\,32^m\,00\overset{s}{.}79$	$-24^\circ\,44'\,46\overset{''}{.}0$	22.8(3)	19.53(8)	17.80(3)

[a]Epoch for astrometry is 1976 May 27. Epoch for photometry is 1993 June 29. Coordinates are accurate to 1 arcsec in RA and Dec.

[b]Numbered stars follow scheme of Doxsey et al. (1977), who also referred to V2116 Oph as GF.

Table 3. Infrared Photometry of V2116 Oph

Date	Telescope	K	$J-H$	$H-K$	$K-L$	$K-L'$	Refs.
1973 May 26	SAAO 1.9-m	8.07(5)	1.54(7)	0.75(7)	···	···	1
1973 Aug 29	SAAO 1.9-m	8.04(5)	1.54(7)	0.70(7)	0.71(7)	···	2
1974 Jun 13	SAAO 1.9-m	8.12(5)	···	0.80(7)	0.63(7)	···	2
1974 Jun 26	SAAO 1.9-m	8.13(5)	···	···	···	···	2
1976 May 22	SAAO 1.9-m	8.03(5)	1.49(7)	0.76(7)	0.74(7)	···	2
1977 Jul 23	SAAO 1.9-m	8.09(5)	1.49(7)	0.74(7)	0.64(7)	···	2
1978 Jun 20	SAAO 1.9-m	7.95(5)	1.51(7)	0.76(7)	0.73(7)	···	2
1980 Mar 23	SAAO 1.9-m	8.05(5)	···	···	···	···	3
1993 Apr 6	Palomar 5-m	8.17(3)	1.57(4)	0.64(4)	···	···	4
1993 Jun 26	SAAO 1.9-m	8.10(2)	1.60(2)	0.61(3)	0.48(4)	···	4
1993 Jun 29	UKIRT 3.8-m	8.17(8)	1.51(3)	0.58(8)	···	0.37(10)	4
1993 Jun 30	UKIRT 3.8-m	8.13(2)	1.48(4)	0.59(4)	···	0.45(8)	4
1993 Jul 1	UKIRT 3.8-m	8.13(2)	1.41(4)	0.49(4)	···	···	4
1993 Jul 6	UKIRT 3.8-m	8.13(2)	1.52(7)	0.44(5)	···	0.42(10)	4
1993 Sep 09	UKIRT 3.8-m	8.06(3)	1.40(6)	0.61(5)	···	···	4
1993 Sep 11	Teide 1.5-m	8.06	1.38	0.62	···	···	4
1994 Jun 30	SAAO 1.9-m	8.16	1.56	0.62	0.50	···	4
1995 Aug 16	SAAO 1.9-m	8.17(1)	1.59(5)	0.63(3)	···	···	4

References. — (1) Glass & Feast 1973; (2) Glass 1979; (3) Glass 1993, personal communication; (4) This work

Table 4. Optical Spectroscopy of V2116 Oph

Date	Telescope	$\lambda\lambda$	$\Delta\lambda$	Ref.	Remarks
1974 Jul 14	Lick 3-m	4600–6700	10	1	Many lines, including [Fe VII]
1975 Jun 13	Lick 3-m	4800–7300	10	1	Many lines, including [Fe VII]
1975 Aug 12	Lick 3-m	5800–8250	10	1	Many lines, including [Fe VII]
1976 Apr 10	AAT 3.8-m	4000–7325	1.3	2	Rich emission line spectrum
1976 Aug 20	AAT 3.8-m	4000–7325	1.3	2,3	Rich emission line spectrum
1983 Aug 7	SAAO 1.9-m	unspecified	···	4	Strong Hα
1983 Nov 4	SAAO 1.9-m	unspecified	···	4	Hα weak or absent
1984 Apr 22	AAT 3.8-m	5200–11000	10	2	Rich emission line spectrum
1988 Mar 21	ANU 2.3-m	unspecified	···	5	Strong Hα
1988 Jun 18,22	WHT 4.2-m	5000–9700	9	6	Many lines
1988 Jul 8	Lick 3-m	4460–7230	2.8	7,8	Rich emission line spectrum
1991 Jul 2	ANU 2.3-m	4000–8500	1.6	9,10	Rich emission line spectrum
1991 Aug 8	Palomar 5-m	3800–5490	2	2	Rich emission line spectrum
1991 Aug 8	Palomar 5-m	5580–6860	1.5	2	Rich emission line spectrum
1991 Aug 9	Palomar 5-m	3800–5490	2	2	Rich emission line spectrum
1991 Aug 9	Palomar 5-m	5580–6860	1.5	2	Rich emission line spectrum
1993 Jun 30	Palomar 5-m	5200–9500	6	2	Rich emission line spectrum
1993 Jul 1	WHT 4.2-m	6200–7000	1.3	2	Hα profile
1993 Sep 10	NTT 3.5-m	6000–9000	3.6	2	Rich emission line spectrum
1993 Sep 10	AAT 3.8-m	5800–7200	1.6	2	He I lines missing
1993 Sep 10	AAT 3.8-m	5800–7200	1.6	2	Rich emission line spectrum
1994 Feb 25	AAT 3.8-m	6300–6850	0.5	2	Hα profile
1994 Mar 7	SAAO 1.9-m	6200–6900	0.5	2	Hα profile
1994 Jul 1	SAAO 1.9-m	6200–6900	0.5	2	Hα profile
1996 Oct 6	SAAO 1.9-m	6200–6900	0.5	2	Strong Hα emission
1996 Oct 16	Mt Stromlo 1.9-m	unspecified	···	11	Hα emission absent
1996 Oct 19	Mt Stromlo 1.9-m	unspecified	···	11	Hα emission absent

References. — (1) Davidsen et al. 1977; (2) This work; (3) Whelan et al. 1977; (4) Whitelock et al. 1983; (5) Dotani et al. 1989; (6) Shahbaz et al. 1996; (7) Gotthelf et al. 1988; (8) Halpern 1994, personal communication; (9) Sood et al. 1991; (10) Sharma et al. 1993; (11) Sood et al. 1996

Table 5. Spectral Classification of V2116 Oph

Date	[VO]	$I(7450)$	$S(7890)$	ST[a]	ST[b]
1975 Aug 12	0.22	0.01	0.63	M4.2	M5
1984 Apr 22	0.28	0.00	0.69	M4.8	M5.5
1993 Jun 30	0.35	0.03	0.84	M5.4	M6
1993 Sep 10	0.12	−0.31	0.30	M3	M3

[a]Spectral type from Kenyon & Fernandez-Castro (1987).

[b]Spectral type from Terndrup et al. (1990).

Table 6. Selected Emission Line Strengths of V2116 Oph

		1974/1975[b]		1976 Apr 10		1976 Aug 20		1988 Jul 8[c]		1993 Jun 30	
λ[a]	Ion	F[d]	I[e]	F[d]	I[e]	F[d]	I[e]	F[d]	I[e]	F[d]	I[e]
4861	H I (Hβ)	2.5	5.9	2.6	6.1	2.6	6.2	1.2	2.9	···	···
4959	[O III]	0.8	1.6	0.5	1.0	0.6	1.2	<2	< 4	···	···
5007	[O III]	1.2	2.3	1.5	2.9	1.1	2.1	4.8	9.3	···	···
5876	He I	3.8	2.8	1.7	1.2	1.5	1.1	2.1	1.5	···	···
6087	[Fe VII]	1.5	0.9	<0.3	<0.2	0.5	0.3	3.3	2.0	···	···
6300	[O I]	0.4	0.2	0.9	0.4	···	···	8.6	4.2	···	···
6563	H I (Hα)	310	121	110	42	72	28	240	94	254	99
6678	He I	5.0	1.8	2.2	0.8	0.9	0.3	3.3	1.2	4.0	1.4
6830	O VI Raman	≈2	≈0.6	0.4	0.1	0.7	0.2	4.2	1.3	···	···
7065	He I	8.3	2.2	1.9	0.5	2.9	0.8	7.5	2.0	6.0	1.6
7281	He I	···	···	1.7	0.4	···	···	···	···	<1	<0.2
7774	O I	5.5	0.9	···	···	···	···	···	···	4.6	0.8
8446	O I	···	···	···	···	···	···	···	···	58	6.9
8498	Ca II	···	···	···	···	···	···	···	···	6.5	0.8
8542	Ca II	···	···	···	···	···	···	···	···	11	1.3
8662	Ca II	···	···	···	···	···	···	···	···	14	1.6

[a]Wavelength (Å)

[b]Average of three spectra (Davidsen, Malina, & Bowyer 1977)

[c]From Gotthelf et al. (1988) and Halpern (1994)

[d]Observed flux in units of 10^{-15} erg cm^{-2} s^{-1}

[e]Dereddened flux in units of 10^{-13} erg cm^{-2} s^{-1}, assuming $A_V = 3.1\,E(B-V) = 5$

Table 7. 1991 August 8 Emission Line Strengths

λ[a]	Ion	F[b]	I[c]	λ[a]	Ion	F[b]	I[c]
3889	H I (H8)	0.53	4.64	5411	He II	0.52	0.62
3970	H I (Hϵ)	0.65	5.16	5425	Fe II (49)	0.99	1.17
4102	H I (Hδ)	0.89	5.90	5755	[N II]	0.78	0.64
4341	H I (Hγ)	1.94	9.22	5876	He I	12.81	9.30
4363	[O III] ?	0.89	4.11	5890	Na I	0.76	0.54
4388	He I ?	0.45	2.02	5895	Na I	0.62	0.45
4416	[Fe II] ?	0.57	2.46	5958	Si II	0.35	0.23
4471	He I	0.32	1.27	5979	Si II	0.47	0.31
4491	Fe II (37)	0.41	1.59	5991	Fe II (46)	0.97	0.63
4555	Fe II ?	0.58	2.04	6084	Fe II (46)	0.54	0.32
4583	Fe II (37)	0.76	2.58	6103	Ca I ?	0.25	0.14
4640	C III/N III	0.91	2.92	6148	Fe II (74)	1.20	0.67
4686	He II	0.72	2.14	6156	O I ?	0.31	0.17
4713	He I	0.43	1.23	6238	Fe II (74)	1.28	0.66
4861	H I (Hβ)	13.45	31.62	6248	Fe II (74)	0.76	0.39
4922	He I ?	1.53	3.32	6300	[O I]	1.76	0.86
4959	[O III]	0.37	0.76	6318	Fe II	1.29	0.62
4994	N II ?	0.41	0.80	6347	Si II	1.81	0.85
5007	[O III]	1.81	3.53	6364	[O I]	1.02	0.47
5016	He I ?	2.14	4.11	6369	Fe II (40)	2.10	0.96
5042	?	0.76	1.42	6384	Fe II	1.21	0.55
5056	Si II ?	0.49	0.90	6407	Fe II (74)	0.11	0.05
5133	Fe II (35)	0.26	0.43	6417	Fe II (74)	0.78	0.34
5158	[Fe II] (18)	0.95	1.53	6433	Fe II (40)	1.95	0.85
5169	Fe II (42)	1.39	2.22	6443	Fe II	0.60	0.26
5184	Mg I	0.26	0.41	6456	Fe II (74)	2.19	0.93
5197	Fe II (49)	0.58	0.90	6482	N II	0.54	0.22
5235	Fe II (49)	0.66	0.97	6491	Fe II	1.05	0.43
5276	?	1.88	2.63	6516	Fe II (40)	4.23	1.71
5317	Fe II (49)	1.40	1.87	6563	H I (Hα)	487.18	189.77
5363	Fe II (48)	0.80	1.01	6678	He I	14.05	4.99
5376	[Fe II] (19)	0.19	0.24	6830	O VI Raman	0.51	0.16

[a]Wavelength (Å)

[b]Observed flux in units of 10^{-15} erg cm^{-2} s^{-1}

[c]Dereddened flux in units of 10^{-13} erg cm^{-2} s^{-1}, assuming $A_V = 3.1\,E(B-V) = 5$

Table 8. 1993 September 10 Emission Line Strengths

		NTT (0133 UT)		AAT (0904 UT)		AAT (0916 UT)	
λ[a]	Ion	F[b]	I[c]	F[b]	I[c]	F[b]	I[c]
5755	[N II]	···	···	0.12	0.10	···	···
5876	He I	···	···	0.73	0.53	5.89	4.27
5890	Na I	···	···	0.41	0.29	0.66	0.47
5895	Na I	···	···	0.21	0.15	0.31	0.22
5958	Si II	···	···	0.19	0.12	0.13	0.09
5979	Si II	···	···	0.14	0.09	<0.1	<0.07
5991	Fe II (46)	···	···	0.28	0.18	0.39	0.26
6084	Fe II (46)	···	···	0.23	0.14	0.32	0.19
6103	Ca I ?	···	···	0.06	0.04	<0.1	<0.06
6148	Fe II (74)	···	···	0.36	0.20	0.53	0.29
6156	O I ?	···	···	0.12	0.06	<0.1	<0.06
6238	Fe II (74)	···	···	0.28	0.14	0.50	0.26
6248	Fe II (74)	···	···	0.47	0.24	0.52	0.26
6300	[O I]	···	···	>0.59	>0.29	0.74	0.36
6318	Fe II	···	···	0.35	0.17	0.50	0.24
6347	Si II	···	···	0.60	0.28	0.74	0.35
6369	Fe II (40)	1.41	0.65	0.59	0.27	1.16	0.534
6384	Fe II	<1.0	<0.45	0.38	0.17	0.60	0.27
6417	Fe II (74)	<1.0	<0.45	0.23	0.10	0.38	0.17
6433	Fe II (40)	0.72	0.32	<0.01	<0.004	0.89	0.39
6443	Fe II	<1.0	<0.4	0.05	0.02	0.17	0.07
6456	Fe II (74)	0.78	0.33	0.61	0.26	0.90	0.38
6482	N II	<1.0	<0.4	0.66	0.28	0.27	0.11
6491	Fe II	<1.0	<0.4	0.24	0.10	0.42	0.17
6516	Fe II (40)	<2.0	<0.3	<0.01	<0.004	1.40	0.57
6563	H I (Hα)	244.62	95.29	>183	>71	310.96	121.13
6678	He I	7.66	2.72	0.53	0.19	6.48	2.30
7002	O I ?	<1.0	<0.3	0.24	0.07	<0.3	<0.08
7065	He I	16.85	4.49	0.29	0.08	12.87	3.43
7115	C II ?	<1.0	<0.3	0.47	0.12	0.47	0.12
7136	[Ar III] ?	<1.0	<0.3	0.40	0.10	0.40	0.10
7155	[Fe II] ?	<1.0	<0.3	0.69	0.17	0.86	0.22
7172	[Fe II] ?	<1.0	<0.3	0.39	0.10	0.34	0.08
7222	Fe II (73)	<1.0	<0.2	0.44	0.11	0.54	0.13

Table 8—Continued

		NTT (0133 UT)		AAT (0904 UT)		AAT (0916 UT)	
λ[a]	Ion	F[b]	I[c]	F[b]	I[c]	F[b]	I[c]
7231	C II ?	<1.0	<0.2	0.84	0.20	1.19	0.28
7281	He I	3.30	0.76	1.31	0.30	2.03	0.47
7291	[Ca II]	<1.0	<0.2	0.57	0.13	0.61	0.14
7308	Fe II (73)	<1.0	<0.2	0.37	0.08	···	···
7712	Fe II (73)	1.39	0.25	···	···	···	···
7774	O I	6.69	1.14	···	···	···	···
8359	H I (Pa22)	3.19	0.40	···	···	···	···
8374	H I (Pa21)	3.09	0.39	···	···	···	···
8392	H I (Pa20)	3.61	0.45	···	···	···	···
8413	H I (Pa19)	5.41	0.66	···	···	···	···
8446	O I	97.24	11.73	···	···	···	···
8467	H I (Pa17)	5.19	0.62	···	···	···	···
8498	Ca II	31.72	3.74	···	···	···	···
8542	Ca II	42.28	4.88	···	···	···	···
8598	H I (Pa14)	3.35	0.38	···	···	···	···
8662	Ca II	30.49	3.34	···	···	···	···
8750	H I (Pa12)	4.95	0.52	···	···	···	···

[a]Wavelength (Å)

[b]Observed flux in units of 10^{-15} erg cm^{-2} s^{-1}

[c]Dereddened flux in units of 10^{-13} erg cm^{-2} s^{-1}, assuming $A_V = 3.1\,E(B-V) = 5$

Table 9. Inferred System Properties for GX 1+4/V2116 Oph

Quantity	FGB mass donor	AGB mass donor
ZAMS donor mass ($M_\odot$)	0.8–2	0.8–10
Donor luminosity ($L_\odot$)	280–1300	4800–8000
Donor radius ($R_\odot$)	50-110	210–270
Distance (kpc)	3–6	12–15
X-ray luminosity (10^{38} erg s^{-1})	0.08–0.3	1–2
Pulsar surface dipole field (G)	$\sim 10^{12}$	$\sim 10^{14}$
Inner disk radius (cm)	$\sim 10^{8}$	$\sim 10^{9}$
Orbital period (d)	$\gtrsim 100$	$\gtrsim 260$

FIGURE CAPTIONS

FIG. 1.— R-band image of the GX 1+4 field, taken on 1993 September 10. The 10.4-arcsec-radius (90%-confidence) *ROSAT* error circle for GX 1+4 is also shown. In addition to V2116 Oph ($R = 16$), a very faint star (NNE, $R = 19.5$) is also visible in the error circle.

FIG. 2.— Optical/near-infrared classification spectra of V2116 Oph. The top panel shows a low-resolution taken on 1993 June 30 from the Palomar 5-m telescope. This spectrum corresponds to spectral type M5.7 III. Due to the wide slit used, most of emission line features are smeared out. The bottom panel shows a higher resolution spectrum taken on 1993 September 3 from the ESO 3.6-m NTT during a bright X-ray outburst. This spectrum corresponds to M3 III.

FIG. 3.— Detailed optical emission line spectrum of V2116 Oph, taken on 1991 August 9 from the Palomar 5-m telescope.

FIG. 4.— Low-resolution infrared spectrum of V2116 Oph in the J, H, and K bands, taken on 1993 April 6 from the Palomar 5-m telescope. The squares shows the corresponding IR photometry points. Also shown is the 1993 June optical spectrum from the top panel of Figure 2. For comparison, the dotted lines shows the best-fit reddened ($A_V = 5$) blackbody curve, corresponding to a color temperature of 2590 K. The blackbody curve is a poor fit to the M giant continuum due to complicated infrared molecular opacities in cool stars.

FIG. 5.— Spectacular rapid line variability in V2116 Oph on 1993 September 10, during a bright X-ray flare. The top panel shows a 900 s exposure centered at 0856 UT. The bottom panel shows a 150 s exposure centered at 0915 UT. The following line features are mostly or completely absent in the first spectrum and clearly present in the second: He I $\lambda\lambda$5876, 6678, 7065, and Fe II $\lambda\lambda$6433, 6516. These lines are indicated by tick marks along the bottom of both panels. The He I λ7281 line is about 50% weaker in the first spectrum. The Hα line was saturated in the first spectrum and so could not be accurately measured. All other line strengths are virtually identical in the two spectra. The bottom panel is representative of the spectrum typically observed.

FIG. 6.— High-resolution Hα spectra from three dates in 1994. The first two spectra were acquired about a week apart, and the third spectrum about 4 months later. The center for all three lines has a velocity around -150 km s^{-1}. A blue wing peak shifted about 150 km

s^{-1} from the center is evident in the first two panels, as is an absorption "notch" blue-shifted about 90 km s−1 from the center.

FIG. 7.— The predicted value for the Iijima K-parameter, the optical emission line diagnostic defined in equation (4), as a function of the inner radius of the accretion disk. The curves shown were computed assuming that the photoionization source is an X-ray heated accretion disk with $r_{\rm out} = 10^{13}$ cm and $\eta_d = 0.9$. The solid curve on the left is for $L_x = 10^{37}$ erg s^{-1}, as appropriate if the mass donor is an FGB star at 3–6 kpc. The solid curve on the right is for $L_x = 10^{38}$ erg s^{-1}, as appropriate if the mass donor is an AGB star at 12–15 kpc. For both curves, various pulsar magnetic field strengths are indicated by tick marks; the corresponding inner disk radius is computed using equation (13). The dotted line indicates the observed value $K = 0.03$. With our simpledisk model, the best solutions consistent with the observed K is $B \approx 5 \times 10^{12}$ G for the FGB case, and $B \approx 7 \times 10^{13}$ G for the AGB case.

Figure 1

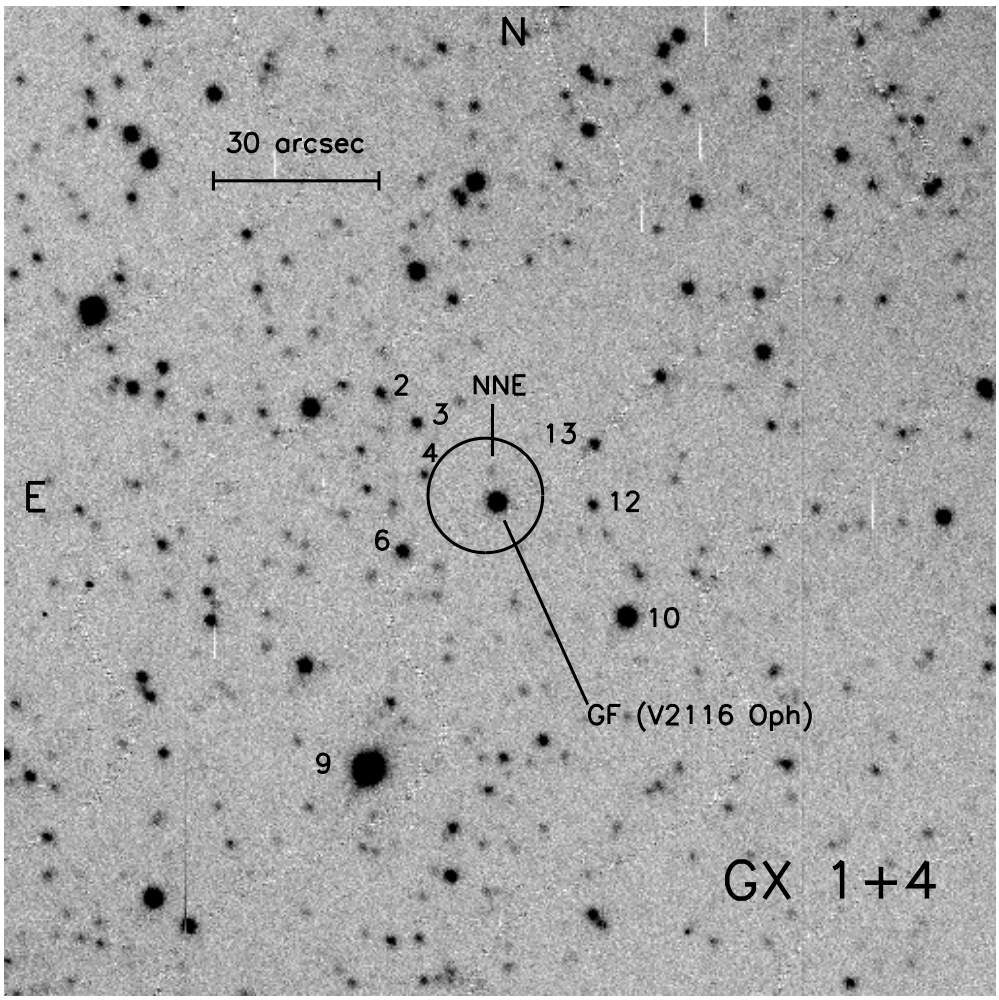

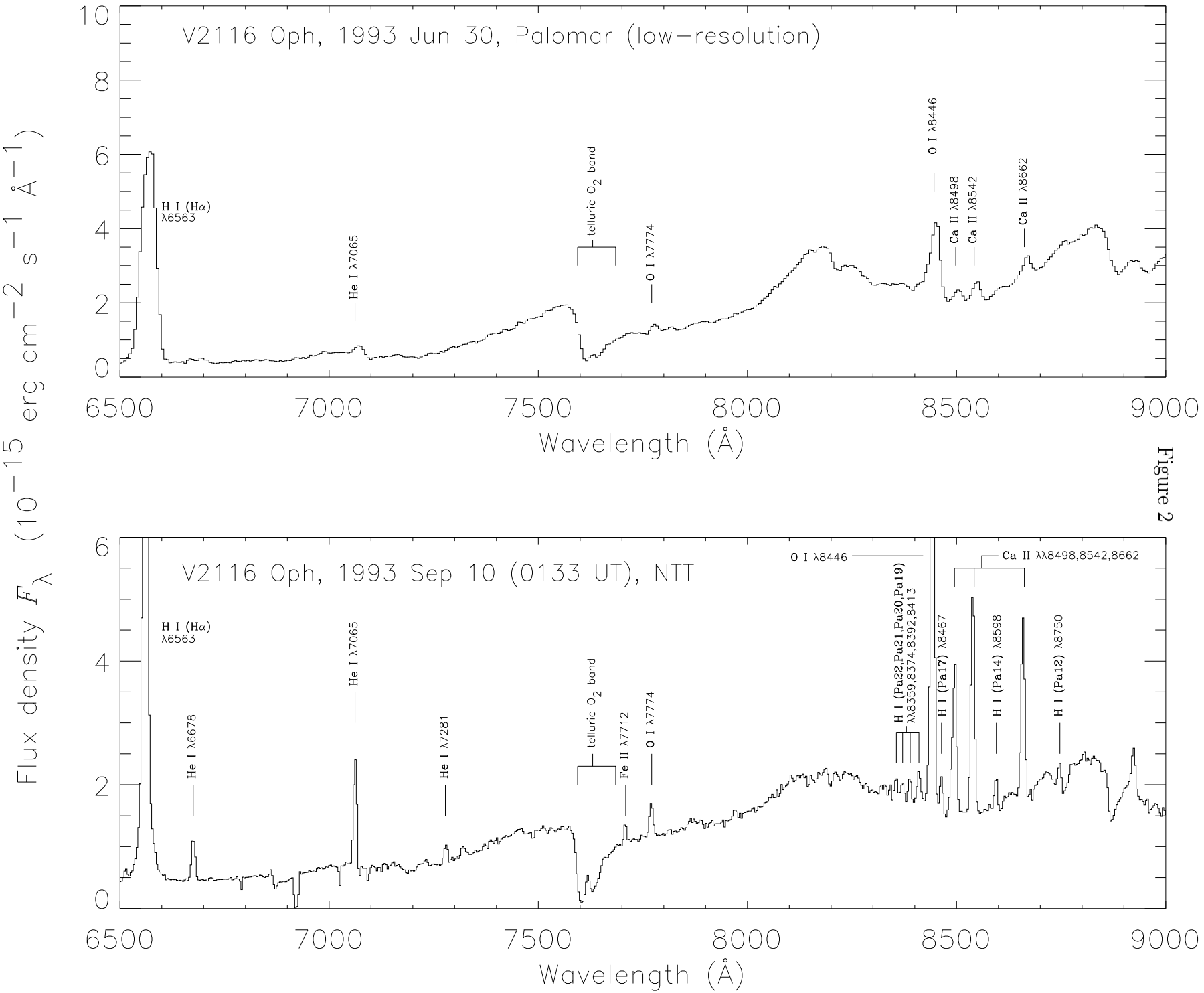
V2116 Oph, 1993 Jun 30, Palomar (low−resolution)
H I (Hα) λ6563
He I λ7065
telluric O2 band
O I λ7774
O I λ8446
Ca II λ8498
Ca II λ8542
Ca II λ8662
V2116 Oph, 1993 Sep 10 (0133 UT), NTT
H I (Hα) λ6563
He I λ6678
He I λ7065
He I λ7281
telluric O2 band
Fe II λ7712
O I λ7774
O I λ8446
H I (Pa22,Pa21,Pa20,Pa19) λλ8359,8374,8392,8413
H I (Pa17) λ8467
H I (Pa14) λ8598
Ca II λλ8498,8542,8662
H I (Pa12) λ8750
Flux density F_λ (10^{-15} erg cm^{-2} s^{-1} Å^{-1})
Wavelength (Å)
0
2
4
6
8
10
6500
7000
7500
8000
8500
9000

Figure 2

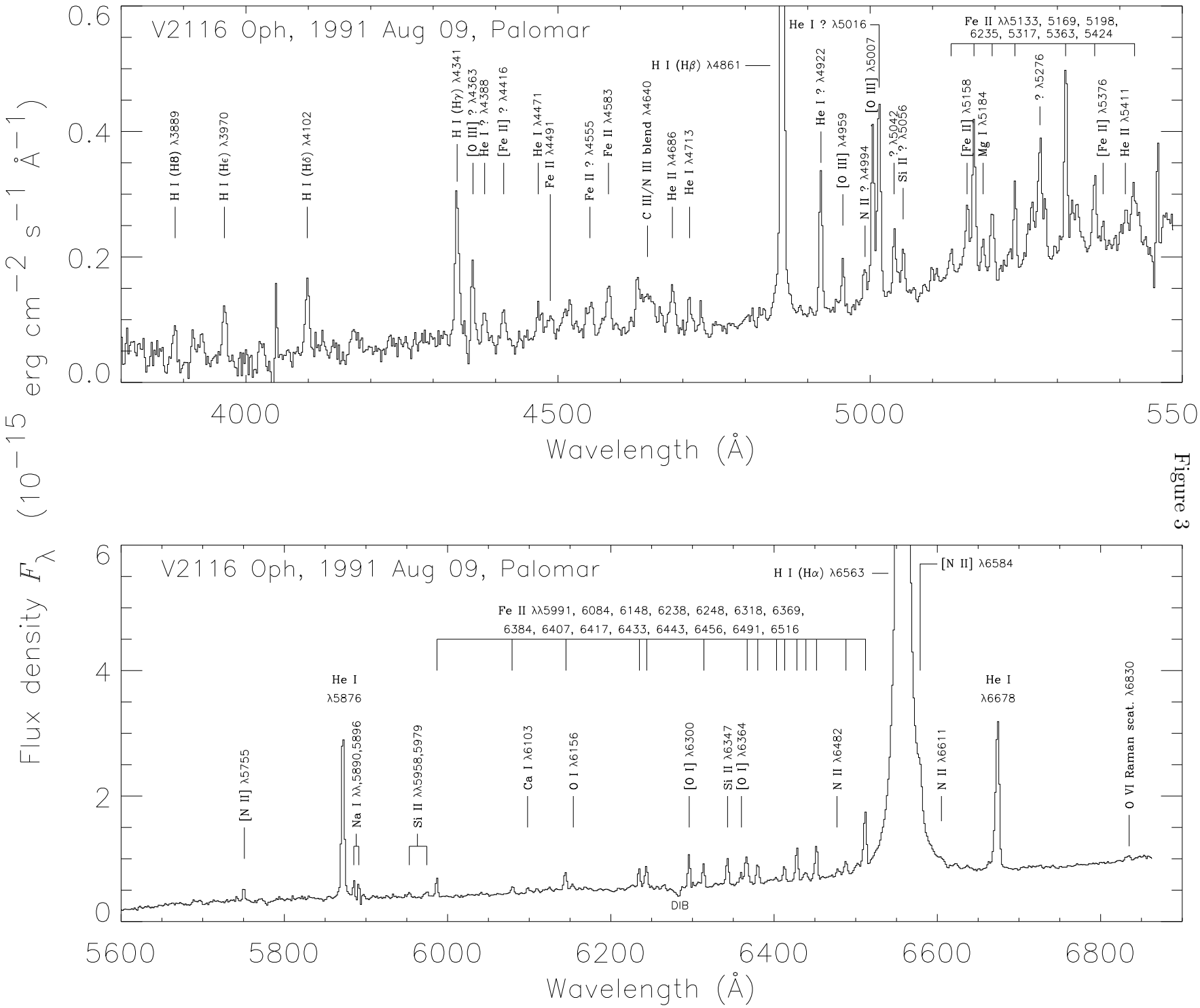
V2116 Oph, 1991 Aug 09, Palomar
Flux density F_λ (10^{-15} erg cm^{-2} s^{-1} Å^{-1})
Wavelength (Å)
H I (H8) λ3889
H I (Hε) λ3970
H I (Hδ) λ4102
H I (Hγ) λ4341
[O III] ? λ4363
He I ? λ4388
[Fe II] ? λ4416
He I λ4471
Fe II λ4491
Fe II ? λ4555
Fe II λ4583
C III/N III blend λ4640
He II λ4686
He I λ4713
H I (Hβ) λ4861
He I ? λ5016
He I ? λ4922
[O III] λ4959
N II ? λ4994
[O III] λ5007
? λ5042
Si II ? λ5056
Fe II λλ5133, 5169, 5198, 6235, 5317, 5363, 5424
[Fe II] λ5158
Mg I λ5184
? λ5276
[Fe II] λ5376
He II λ5411
V2116 Oph, 1991 Aug 09, Palomar
Flux density F_λ
Wavelength (Å)
[N II] λ5755
He I λ5876
Na I λλ,5890,5896
Si II λλ5958,5979
Ca I λ6103
O I λ6156
[O I] λ6300
Si II λ6347
[O I] λ6364
N II λ6482
H I (Hα) λ6563
[N II] λ6584
N II λ6611
He I λ6678
O VI Raman scat. λ6830
Fe II λλ5991, 6084, 6148, 6238, 6248, 6318, 6369, 6384, 6407, 6417, 6433, 6443, 6456, 6491, 6516
DIB

Figure 3

Figure 4

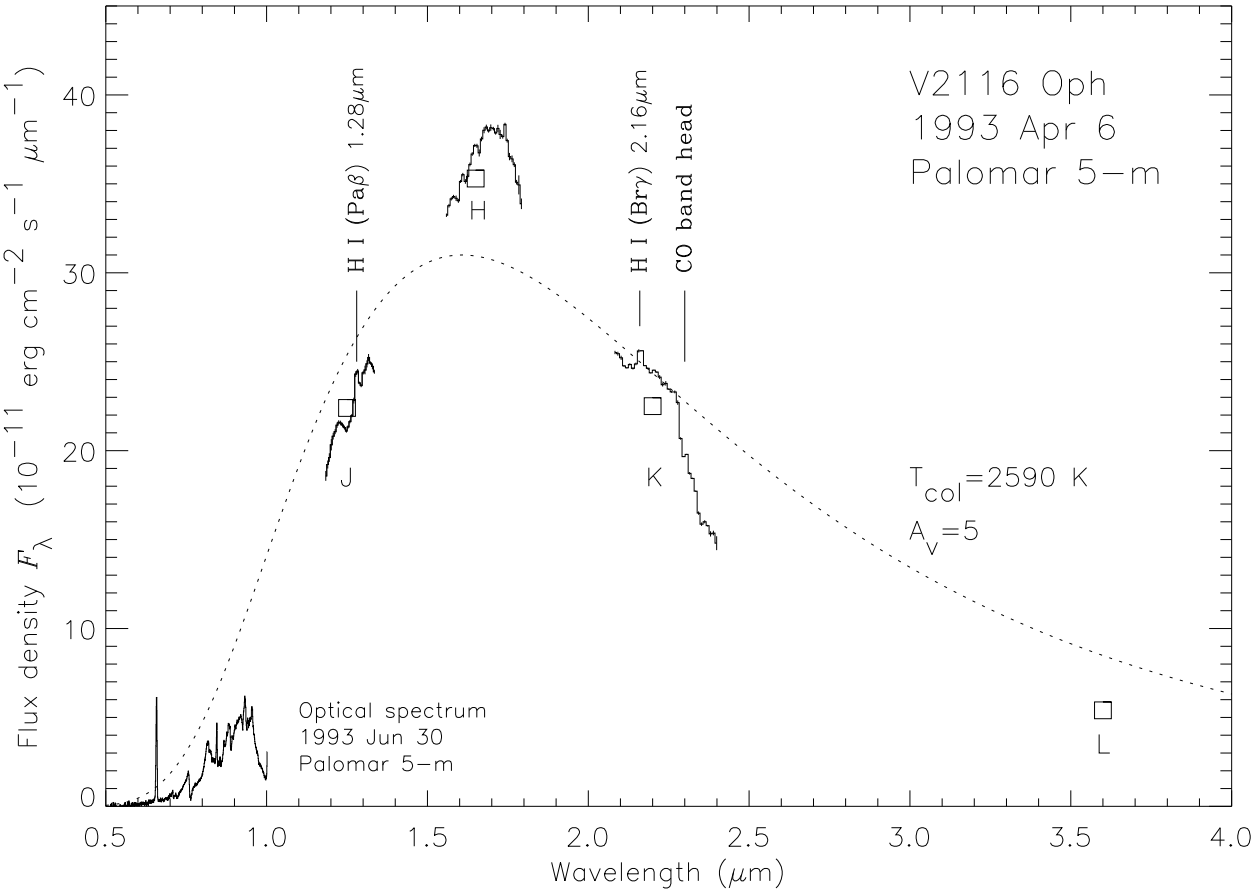
V2116 Oph
1993 Apr 6
Palomar 5−m
H I (Paβ) 1.28μm
H I (Brγ) 2.16μm
CO band head
J
H
K
L
T_col=2590 K
A_V=5
Optical spectrum
1993 Jun 30
Palomar 5−m
Flux density F_λ (10^−11 erg cm^−2 s^−1 μm^−1)
Wavelength (μm)
0
10
20
30
40
0.5
1.0
1.5
2.0
2.5
3.0
3.5
4.0

Figure 5

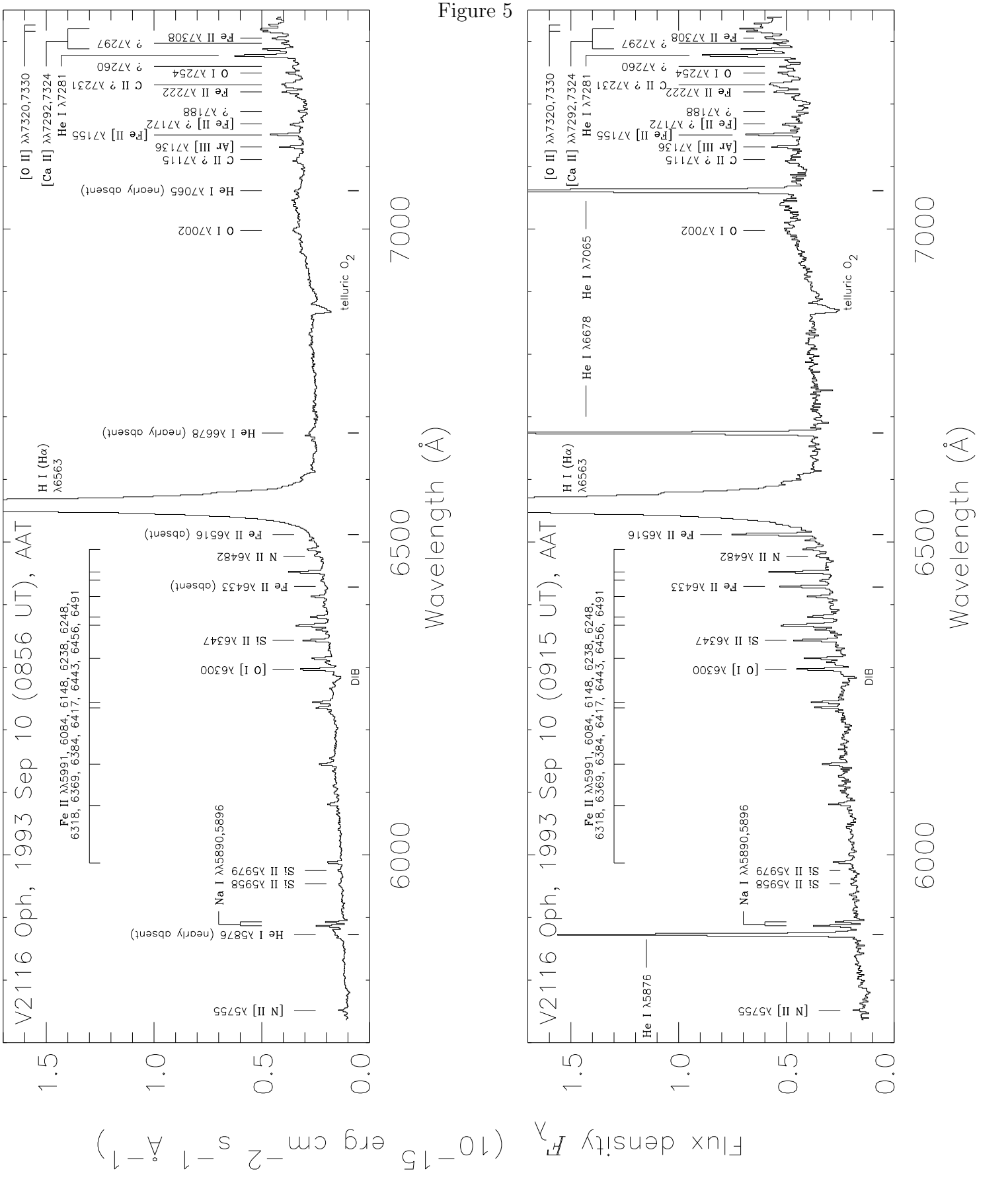
V2116 Oph, 1993 Sep 10 (0856 UT), AAT
V2116 Oph, 1993 Sep 10 (0915 UT), AAT
Flux density F_λ (10^{-15} erg cm^{-2} s^{-1} Å^{-1})
Wavelength (Å)
6000
6500
7000
0.0
0.5
1.0
1.5
[O II] λλ7320,7330
[Ca II] λλ7292,7324
He I λ7281
H I (Hα) λ6563
He I λ6678
He I λ7065
O I λ7002
telluric O_2
C II ? λ7115
[Ar III] λ7136
[Fe II] λ7155
[Fe II] ? λ7172
? λ7188
Fe II λ7222
C II ? λ7231
O I λ7254
? λ7260
Fe II λ7308
? λ7297
[N II] λ5755
He I λ5876
Na I λλ5890,5896
Si II λ5958
Si II λ5979
Fe II λλ5991, 6084, 6148, 6238, 6248, 6318, 6369, 6384, 6417, 6443, 6456, 6491
[O I] λ6300
Si II λ6347
Fe II λ6433
N II λ6482
Fe II λ6516
DIB

Figure 6

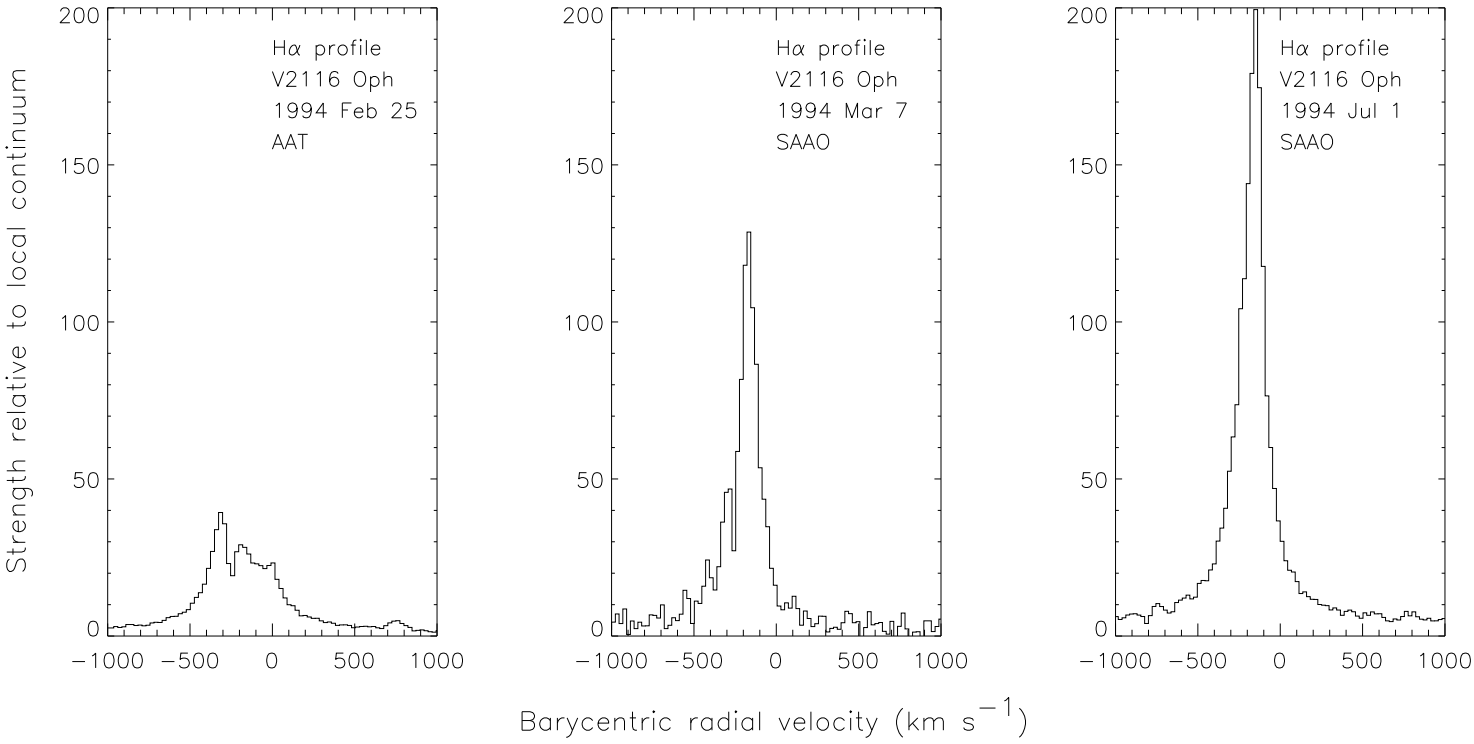
Hα profile
V2116 Oph
1994 Feb 25
AAT
Hα profile
V2116 Oph
1994 Mar 7
SAAO
Hα profile
V2116 Oph
1994 Jul 1
SAAO
Strength relative to local continuum
Barycentric radial velocity (km s^{-1})
0
50
100
150
200
−1000
−500
0
500
1000

Figure 7

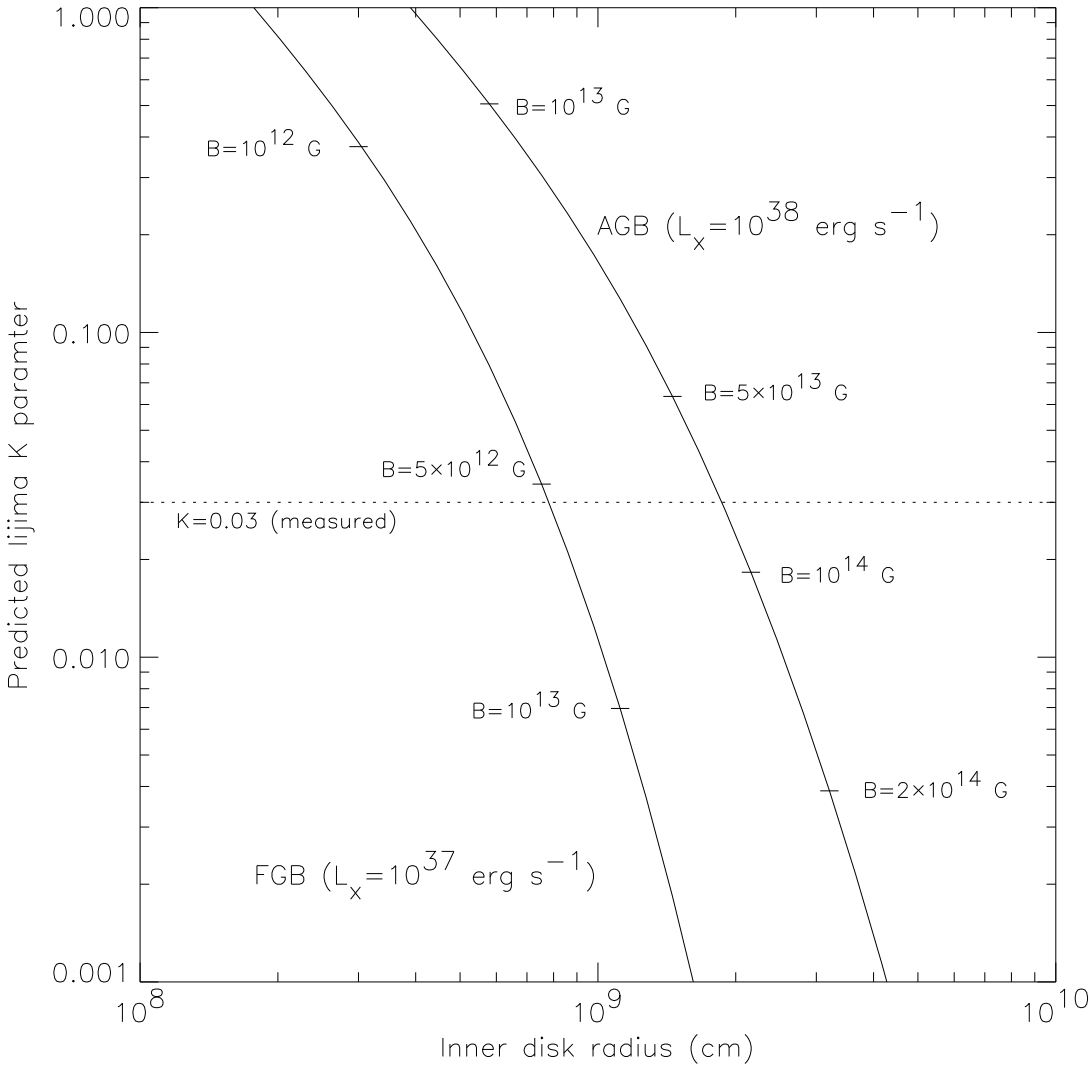
1.000
0.100
0.010
0.001
Predicted Iijima K paramter
10^8
10^9
10^{10}
Inner disk radius (cm)
B=10^{12} G
B=10^{13} G
AGB (L_x=10^{38} erg s^{-1})
B=5×10^{13} G
B=5×10^{12} G
K=0.03 (measured)
B=10^{14} G
B=10^{13} G
B=2×10^{14} G
FGB (L_x=10^{37} erg s^{-1})